Supplementary Information

Unveiling n→π* Interactions: Convergence of Quantum Crystallography and Computational Insights

Alvaro Polo, Pilar García-Orduña, Jorge Echeverría, and Pablo J. Sanz Miguel*

Departamento de Química Inorgánica, Instituto de Síntesis Química y Catálisis Homogénea (ISQCH), Universidad de Zaragoza-CSIC, 50009 Zaragoza, Spain

Table of contents

1. General methods and materials

All the reagents used in this work were purchased from commercial sources and used as received. Glassware was dried at 120 °C before use. Unless otherwise stated, all reactions were carried out under aerobic conditions. Organic solvents were dried by standard procedures and distilled under argon prior to use, or obtained oxygen- and waterfree from a Solvent Purification System (Innovative Technologies). ^{1}H and ^{13}C{^{1}H} NMR spectra were recorded on Bruker Avance 300 (300.13 and 75.48 MHz, respectively) and Bruker Avance 400 (400.16 and 100.61 MHz, respectively) spectrometers. Spectral assignments were achieved by combination of ^{1}H-^{1}H COSY, ^{13}C{^{1}H}-APT and ^{1}H-^{13}C HSQC/HMBC. NMR chemical shifts (expressed in parts per million) are referenced to residual solvent peaks (^{1}H and ^{13}C). Methanol was used as internal standard in ^{13}C{^{1}H} and ^{1}H-^{13}C HSQC/HMBC spectra carried out in D_2O. Coupling constants, *J*, are given in hertz (Hz). High-resolution electrospray mass spectra (HRMS) were acquired using a MicroTOF-Q hybrid quadrupole time-of-flight spectrometer (Bruker Daltonics, Bremen, Germany).

2. Experimental section and spectroscopic details

Synthesis of 1[NO$_3$]: **1**[NO$_3$] was synthesized with slight modifications of a previously published method.[SI-1] Caffeine (8.00 g, 41.2 mmol) was added to an aqueous solution (100 mL) of sodium hydroxide (5.06 g, 126 mmol) and stirred for 24 hours. The white precipitate gradually disappeared, leading to a colorless solution. At 0 °C, nitric acid (15 mL, 237 mmol) was added dropwise and the mixture stirred for 30 minutes. The white precipitate was filtered, washed with small portions of water and cold methanol and dried under vacuum to yield 3.30 g (14.3 mmol, 35%) of **1**[NO$_3$]. ^{1}H NMR (400 MHz, DMSO-d_6, 298 K): δ 8.72 (s, 1H, *C8*-H), 7.60 (d, $^{3}J_{H-H}$ = 4.5 Hz, 1H, *N1*-H), 3.87 (s, 3H, *N7*-CH$_3$), 2.83 (s, 3H, *N3*-CH$_3$), 2.73 (d, $^{3}J_{H-H}$ = 4.5 Hz, 3H, *N1*-CH$_3$). ^{13}C{^{1}H} NMR (100 MHz, DMSO-d_6, 298 K): δ 159.4 (C6), 143.8 (C4), 131.6 (C8), 105.0 (C5), 36.0 (*N7*-C), 30.3 (*N3*-C), 26.0 (*N1*-C). HRMS (DMSO/MeOH) [M – NO$_3$ – H + Na]$^{+}$ calcd. for $C_7H_{12}N_4ONa$: 191.0903; Found: 191.0906.

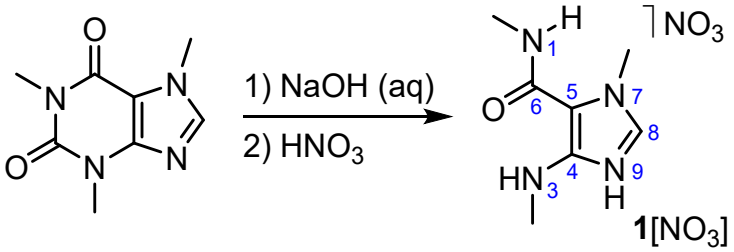

Figure SI-1. Synthesis of **1**[NO$_3$].

Synthesis of 2[NO$_3$]: **2**[NO$_3$] was synthesized with slight modifications of a previously published procedure.[SI-2] A suspension of **1**[NO$_3$] (2.70 g, 11.7 mmol) in 15 mL of triethyl orthoformate was stirred at 110 °C for 90 minutes. Once the mixture cooled down to room temperature, acetone (10 mL) was added and the white solid was filtered off, washed with small portions of acetone and dried under vacuum to yield 1.96 g (8.14 mmol, 70%) of **2**[NO$_3$]. Crystals suitable for X-ray diffraction analysis were grown by slow diffusion of diethyl ether into a solution of **2**[NO$_3$] in acetonitrile at 4 °C. ^{1}H NMR (400 MHz, DMSO-d_6, 298 K): δ 9.82 (s, 1H, *C2*-H), 8.57 (s, 1H, *C8*-H), 4.05 (s, 3H, *N7*-CH$_3$), 3.98 (s, 3H, *N3*-CH$_3$), 3.64 (s, 3H, *N1*-CH$_3$). ^{13}C{^{1}H} NMR (100 MHz, DMSO-d_6,

298 K): δ 151.5 (C6), 151.3 (C2), 147.2 (C8), 146.2 (C4, C8), 114.4 (C5), 37.3 (*N3*-C), 35.6 (*N1*-C), 33.8 (*N7*-C). HRMS (MeOH) $[M - NO_3]^+$ calcd. for $C_8H_{11}N_4O$: 179.0927; Found: 179.0936.

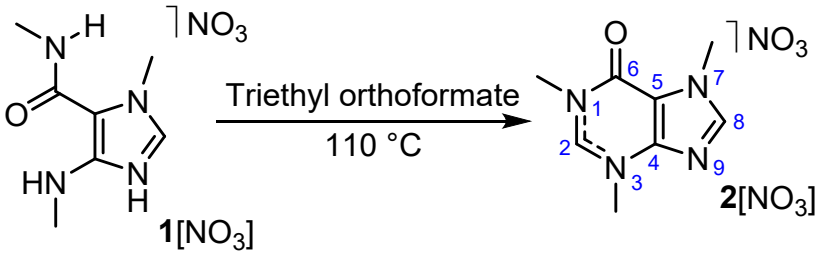

Figure SI-2. Synthesis of **2**[NO_3].

Synthesis of 1[Cl]: **1**[NO_3] (2.42 g, 10.5 mmol) was added to an aqueous solution (12 mL) of potassium carbonate (3.62 g, 26.2 mmol) and the mixture stirred for 30 minutes. The grey oil which separated was extracted three times into chloroform (3 × 10 mL). The organic phases were combined, washed with magnesium sulfate and evaporated to dryness, obtaining a dense yellow oil. Shortly after, the oil was dissolved in 8 mL of acetone and 1.6 mL (19 mmol) of hydrochloric acid (37%) were added, giving rise to a white precipitate, which was filtered, washed with small portions of acetone and dried under vacuum to yield 1.26 g of **1**[Cl] (6.16 mmol, 59%). Crystals suitable for X-ray diffraction analysis were grown by slow diffusion of diethyl ether into a solution of **1**[Cl] in methanol at 4 °C. ^{1}H NMR (400 MHz, CD_3OD, 298 K): δ 8.58 (s, 1H, *C8*-H), 3.99 (s, 3H, *N7*-CH_3), 2.97 (s, 3H, *N3*-CH_3), 2.87 (s, 3H, *N1*-CH_3). ^{13}C{^{1}H} NMR (100 MHz, CD_3OD, 298 K): δ 161.6 (C6), 145.3 (C4), 133.3 (C8), 106. (C5), 36.9 (*N7*-C), 30.8 (*N3*-C), 26.4 (*N1*-C). HRMS (MeOH) $[M - Cl]^+$ calcd. for $C_7H_{13}N_4O$: 169.1084; Found: 169.1090.

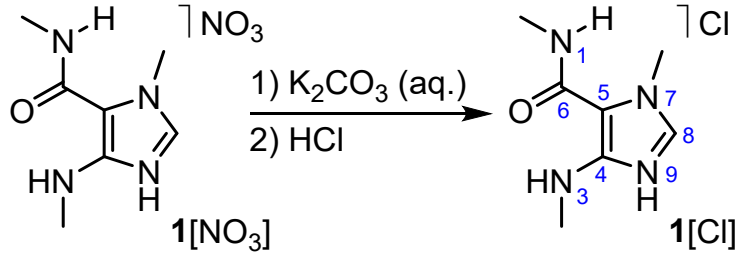

Figure SI-3. Synthesis of **1**[Cl].

Synthesis of 2[Cl]: **1**[Cl] (993 mg, 4.85 mmol) was suspended in triethyl orthoformate (7 mL) and the mixture heated at 110 °C for 2 hours. After cooling down to room temperature, 5 mL of acetone were added and the white precipitate was filtered, washed with small portions of acetone and dried under vacuum to yield 996 mg (4.64 mmol, 96%) of **2**[Cl]. Crystals suitable for X-ray diffraction analysis were grown by slow evaporation of a saturated solution of **2**[Cl] in water at room temperature. ^{1}H NMR (400 MHz, CD_3OD, 298 K): δ 9.69 (s, 1H, *C2*-H), 8.37 (s, 1H, *C8*-H), 4.15 (s, 3H, *N7*-CH_3), 4.11 (s, 3H, *N3*-CH_3), 3.78 (s, 3H, *N1*-CH_3). ^{13}C{^{1}H} NMR (100 MHz, CD_3OD, 298 K): δ 152.9 (C6), 151.9 (t, $^1J_{C-D}$ = 32.5 Hz, C2), 147.8 (C4), 147.3 (C8), 116.4 (C5), 38.2 (*N3*-C), 36.8 (*N1*-C), 34.5 (*N7*-C). HRMS (MeOH) $[M - Cl]^+$ calcd. for $C_8H_{11}N_4O$: 179.0927; Found: 179.0936.

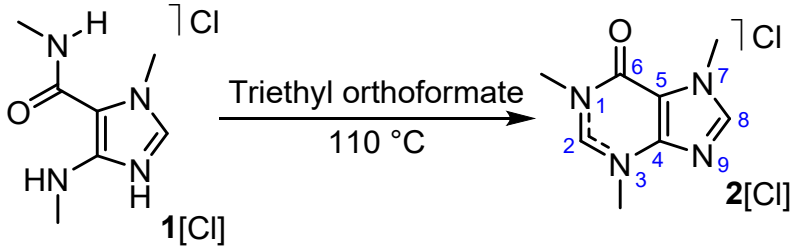

Figure SI-4. Synthesis of **2**[Cl].

Synthesis of 2[PF_6]: **2**[PF_6] was synthesized with slight modifications of a previously published procedure.[SI-2] Ammonium hexafluorophosphate (435 mg, 2.67 mmol) was added to a solution of **2**[NO_3] (615 mg, 2.55 mmol) in water (10 mL). After vigorous stirring for 15 minutes, the white precipitate was filtered off, washed with small portions of water and cold methanol and dried under vacuum to yield 658 mg (2.03 mmol, 80%) of **2**[PF_6]. ^{1}H NMR (400 MHz, CD_3CN, 298 K): δ 8.94 (s, 1H, *C2*-H), 8.12 (s, 1H, *C8*-H), 4.05 (s, 3H, *N7*-CH_3), 4.00 (s, 3H, *N3*-CH_3), 3.67 (s, 3H, *N1*-CH_3). ^{13}C{^{1}H} NMR (100 MHz, CD_3CN, 298 K): δ 152.5 (C6), 150.9 (C2), 147.5 (C4), 147.0 (C8), 116.3 (C5), 38.5 (*N3*-C), 36.6 (*N1*-C), 34.8 (*N7*-C). HRMS (CH_3CN) [M – PF_6]$^+$ calcd. for $C_8H_{11}N_4O$: 179.0927; Found: 179.0927.

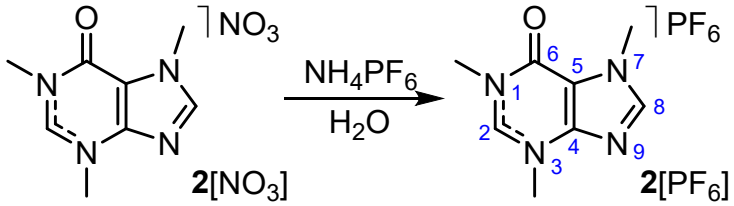

Figure SI-5. Synthesis of **2**[PF_6].

Synthesis of 2[Br]: lithium bromide (374 mg, 4.31 mmol) was added to a solution of **2**[PF_6] (528 mg, 1.63 mmol) in acetonitrile (5 mL). After vigorous stirring for 10 minutes, the white precipitate was filtered off, washed with small portions of diethyl ether and acetone and dried under vacuum to yield 341 mg (1.32 mmol, 81%) of **2**[Br]. Crystals suitable for X-ray diffraction analysis were grown by slow evaporation of a saturated solution of **2**[Br] in water at room temperature. ^{1}H NMR (400 MHz, DMSO-d_6, 298 K): δ 10.03 (s, 1H, *C2*-H), 8.60 (s, 1H, *C8*-H), 4.05 (s, 3H, *N7*-CH_3), 3.98 (s, 3H, *N3*-CH_3), 3.64 (s, 3H, *N1*-CH_3). ^{13}C{^{1}H} NMR (100 MHz, DMSO-d_6, 298 K): δ 151.6 (C6), 151.0 (C2), 146.2 (C8, C4), 114.4 (C5), 37.2 (*N3*-C), 35.4 (*N1*-C), 33.8 (*N7*-C). HRMS (MeOH) [M – Br]$^+$ calcd. for $C_8H_{11}N_4O$: 179.0927; Found: 179.0934.

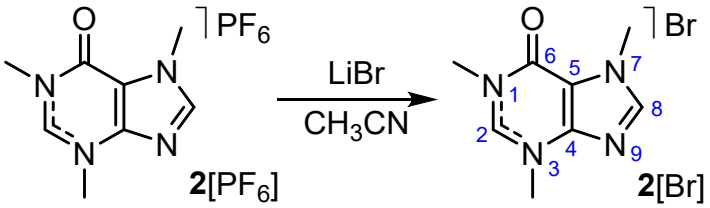

Figure SI-6. Synthesis of **2**[Br].

Synthesis of 2[I]: sodium iodide (930 mg, 6.20 mmol) was added to a solution of **2**[PF_6] (798 mg, 2.46 mmol) in acetonitrile (6 mL). After vigorous stirring for 20 minutes, the yellow precipitate was filtered off, washed with small portions of diethyl ether and acetone and dried under vacuum to yield 641 mg (2.09 mmol, 85%) of **2**[I]. Crystals suitable for X-ray diffraction analysis

were grown by slow evaporation of a saturated solution of **2**[I] in water at room temperature. ^{1}H NMR (400 MHz, DMSO-d_6, 298 K): δ 9.85 (s, 1H, *C2*-H), 8.58 (s, 1H, *C8*-H), 4.05 (s, 3H, *N7*-CH_3), 3.97 (s, 3H, *N3*-CH_3), 3.63 (s, 3H, *N1*-CH_3). ^{13}C{^{1}H} NMR (100 MHz, DMSO-d_6, 298 K): δ 151.5 (C6), 151.0 (C2), 146.1 (C8, C4), 114.4 (C5), 37.3 (*N3*-C), 35.5 (*N1*-C), 33.8 (*N7*-C). HRMS (MeOH) [M – I]$^{+}$ calcd. for $C_8H_{11}N_4O$: 179.0927; Found: 179.0931.

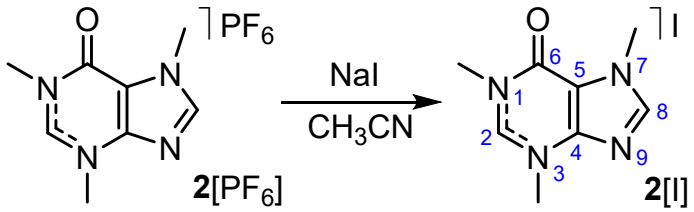

Figure SI-7. Synthesis of **2**[I].

Synthesis of 3[Cl]: **1**[Cl] (842 mg, 4.11 mmol) was suspended in triethyl orthoacetate (4 mL) and the mixture heated at 110 °C for 2 hours. After cooling down to room temperature, 10 mL of acetone were added and the white precipitate was filtered, washed with small portions of acetone and dried under vacuum to yield 738 mg (3.23 mmol, 57%) of **3**[Cl]. Crystals suitable for X-ray diffraction analysis were grown by slow evaporation of a saturated solution of **3**[Cl] in water at room temperature. ^{1}H NMR (400 MHz, D_2O, 298 K): δ 8.29 (s, 1H, *C8*-H), 4.16 (s, 1H, *N3*-CH_3), 4.11 (s, 3H, *N7*-CH_3), 3.81 (s, 3H, *N1*-CH_3), 3.02 (s, 3H, *C2*-CH_3).^{13}C{^{1}H} NMR (100 MHz, D_2O, 298 K): δ 161.7 (C2), 153.2 (C6), 147.4 (C4), 146.7 (C8), 114.8 (C5), 37.1 (*N3*-C), 34.6 (*N7*-C), 33.7 (*N1*-C), 19.4 (*C2*-C). HRMS (MeOH) [M – Cl]$^{+}$ calcd. for $C_9H_{13}N_4O$: 193.1084; Found: 193.1092.

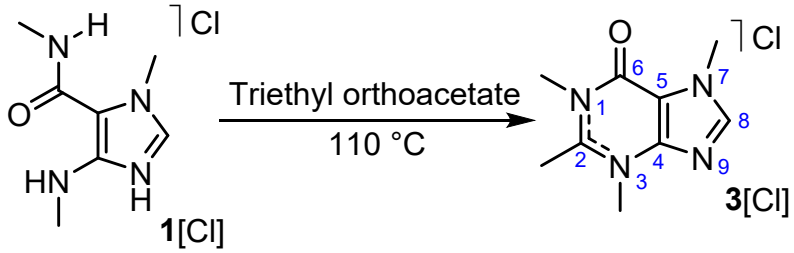

Figure SI-8. Synthesis of **3**[Cl].

3. NMR spectra

NMR spectra of 1[NO_3]

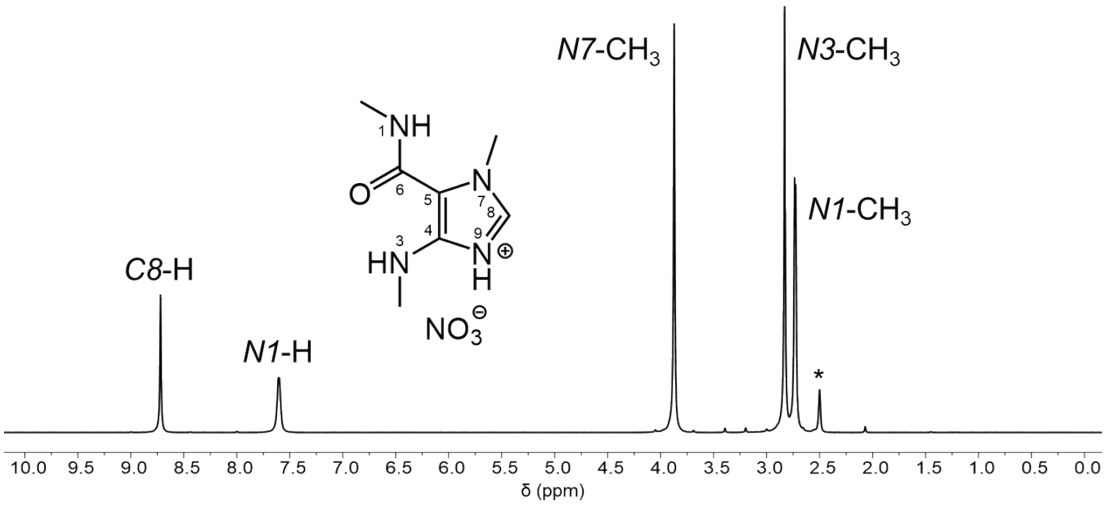

Figure SI-9. ^{1}H NMR spectrum of **1**[NO_3] in DMSO-d_6 at 298 K.

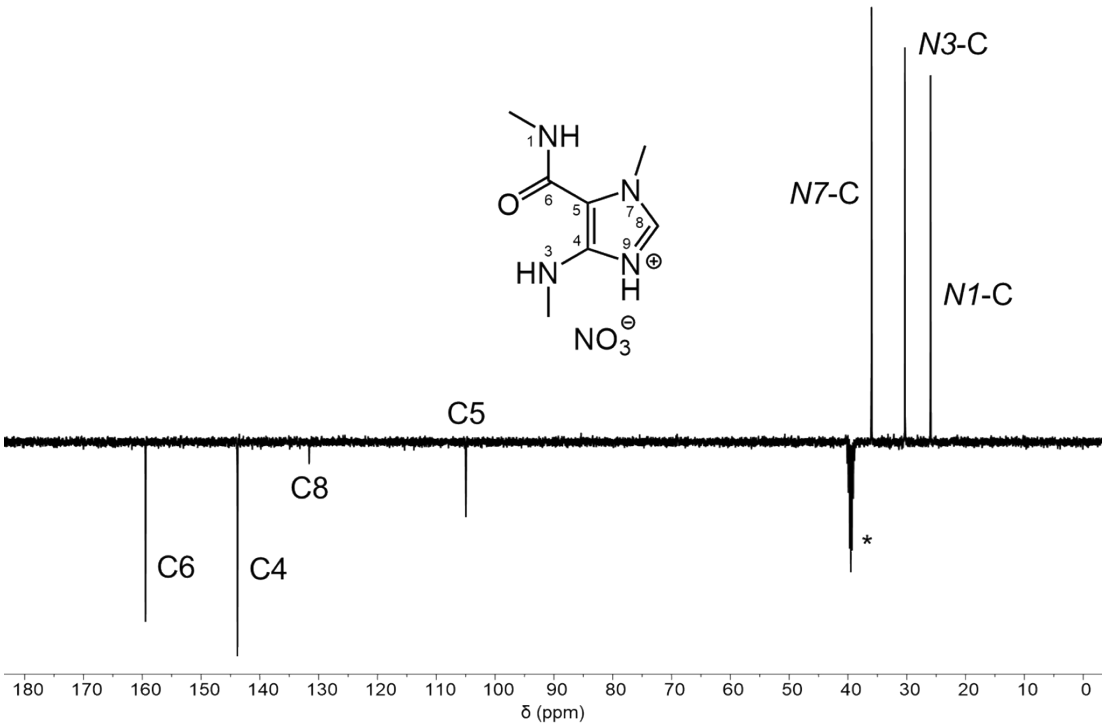

Figure SI-10. ^{13}C{^{1}H}-APT NMR spectrum of **1**[NO_3] in DMSO-d_6 at 298 K.

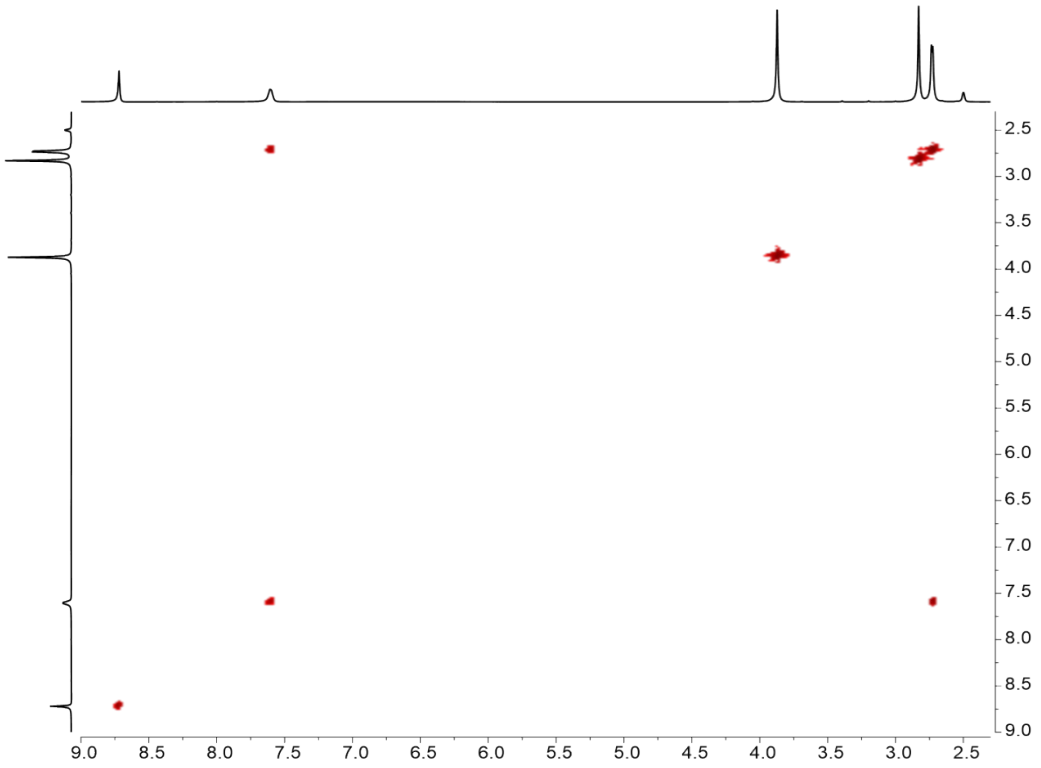

Figure SI-11. ^{1}H-^{1}H COSY NMR spectrum of **1**[NO_3] in DMSO-d_6 at 298 K.

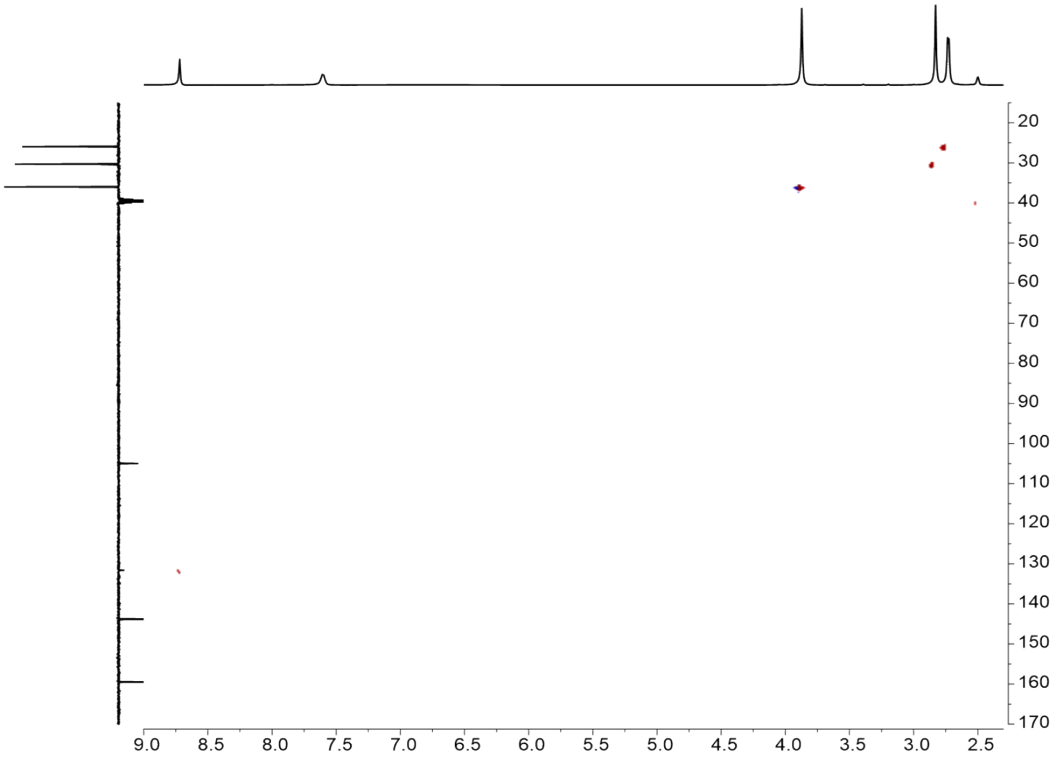

Figure SI-12. ^{1}H-^{13}C HSQC NMR spectrum of **1**[NO_3] in DMSO-d_6 at 298 K.

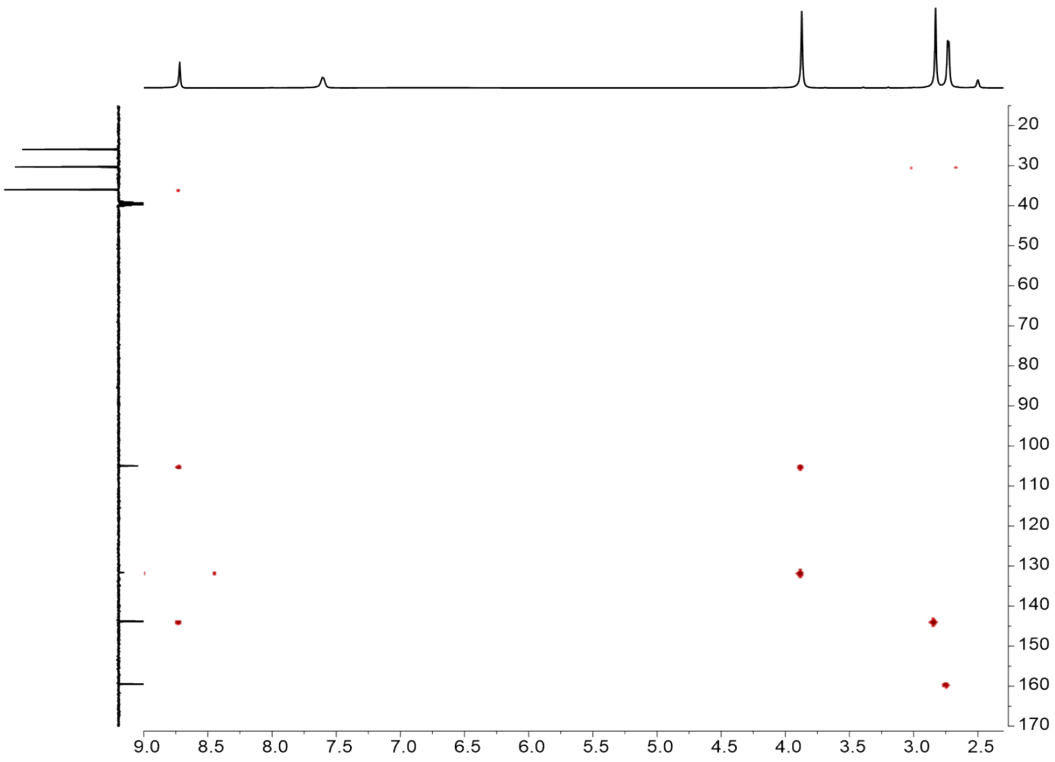

Figure SI-13. ^{1}H-^{13}C HMBC NMR spectrum of **1**[NO_3] in DMSO-d_6 at 298 K.

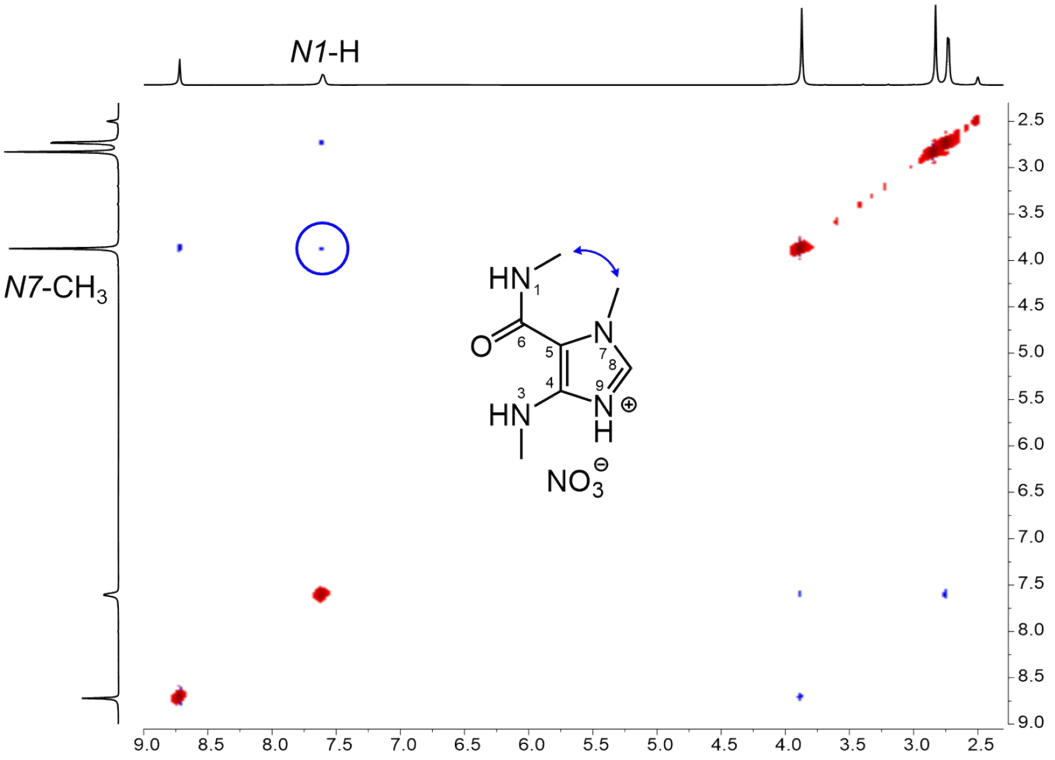

Figure SI-14. ^{1}H-^{1}H 2D-NOESY NMR spectrum of **1**[NO_3] in DMSO-d_6 at 298 K.

NMR spectra of 2[NO_3]

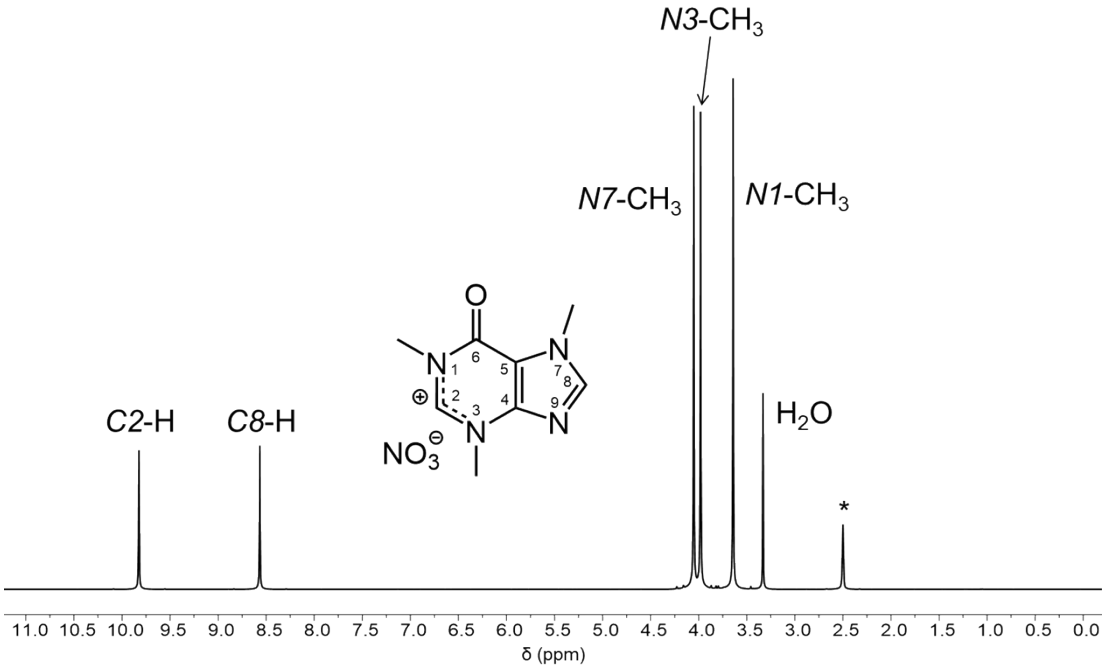

Figure SI-15. ^{1}H NMR spectrum of **2**[NO_3] in DMSO-d_6 at 298 K.

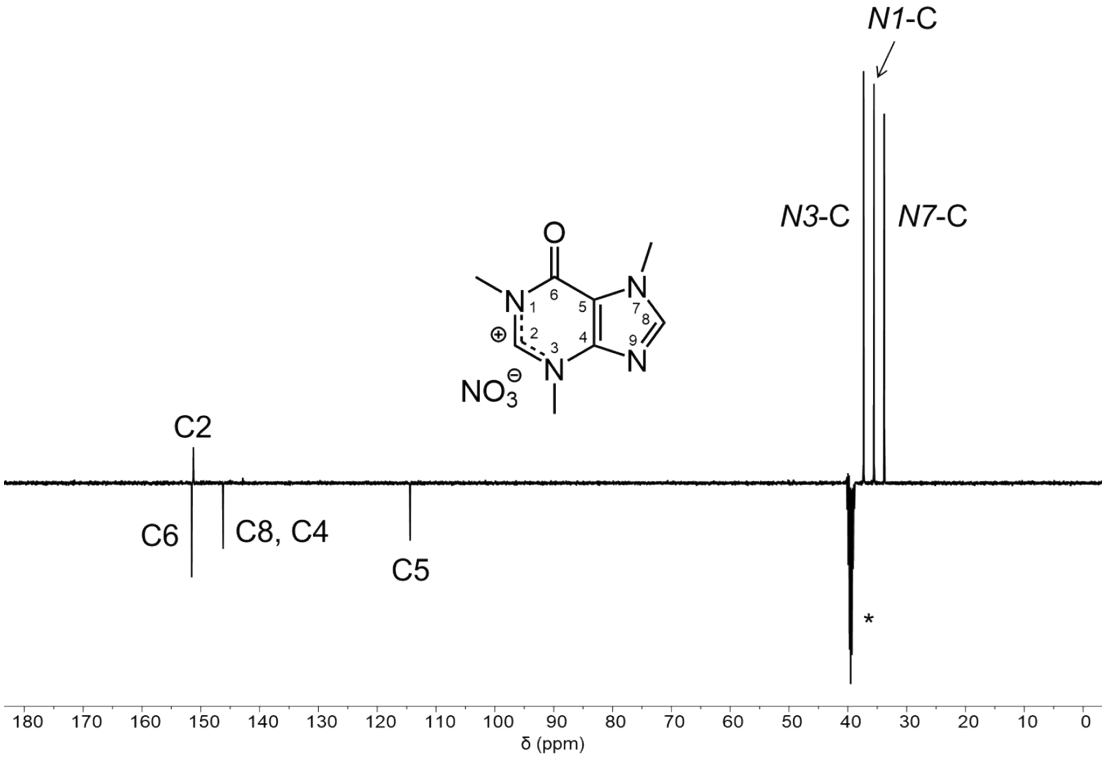

Figure SI-16. ^{13}C{^{1}H}-APT NMR spectrum of **2**[NO_3] in DMSO-d_6 at 298 K.

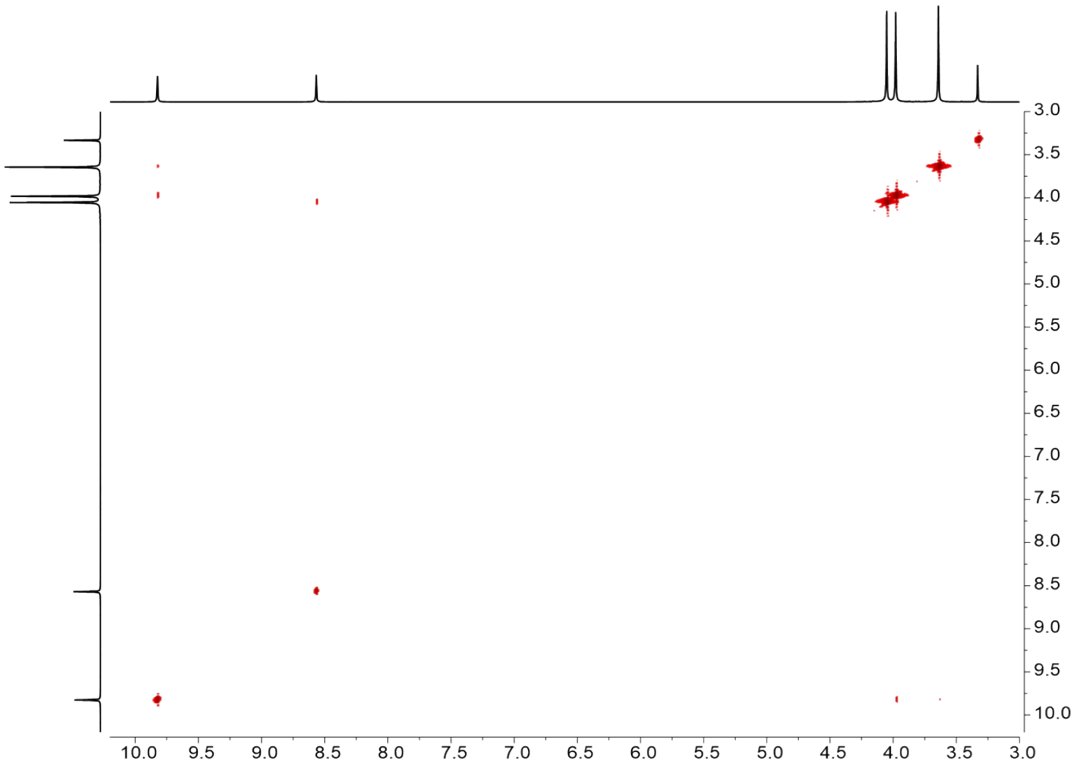

Figure SI-17. ^{1}H-^{1}H COSY NMR spectrum of **2**[NO_3] in DMSO-d_6 at 298 K.

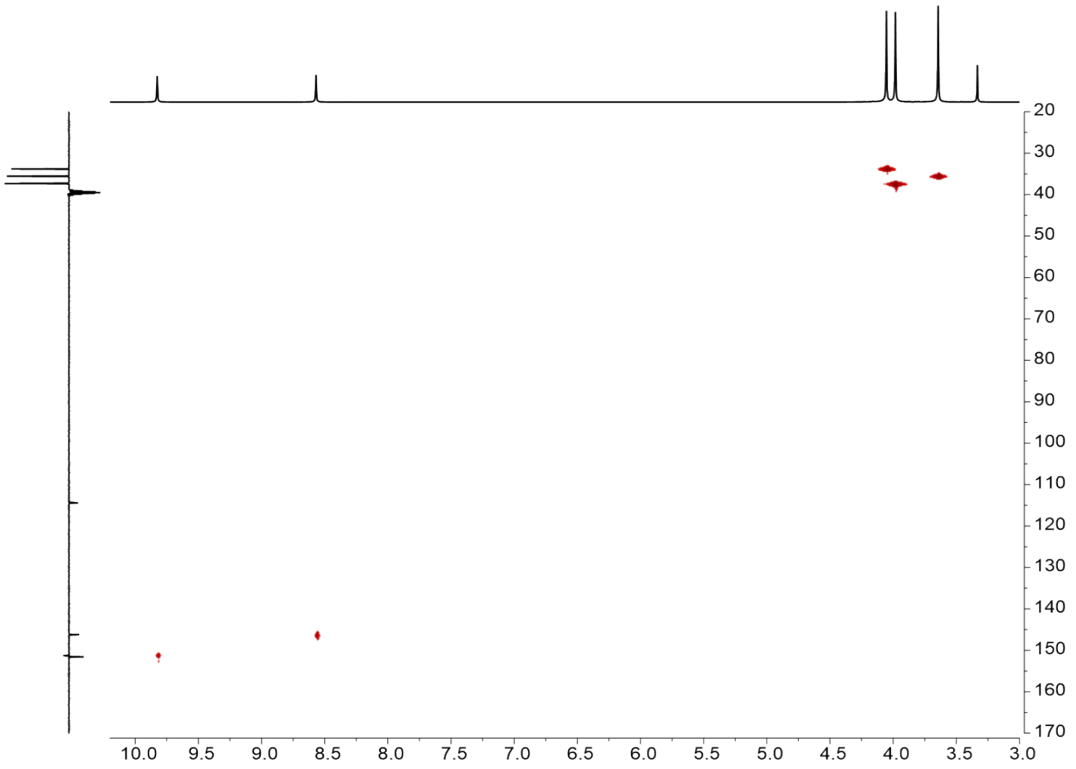

Figure SI-18. ^{1}H-^{13}C HSQC NMR spectrum of **2**[NO_3] in DMSO-d_6 at 298 K.

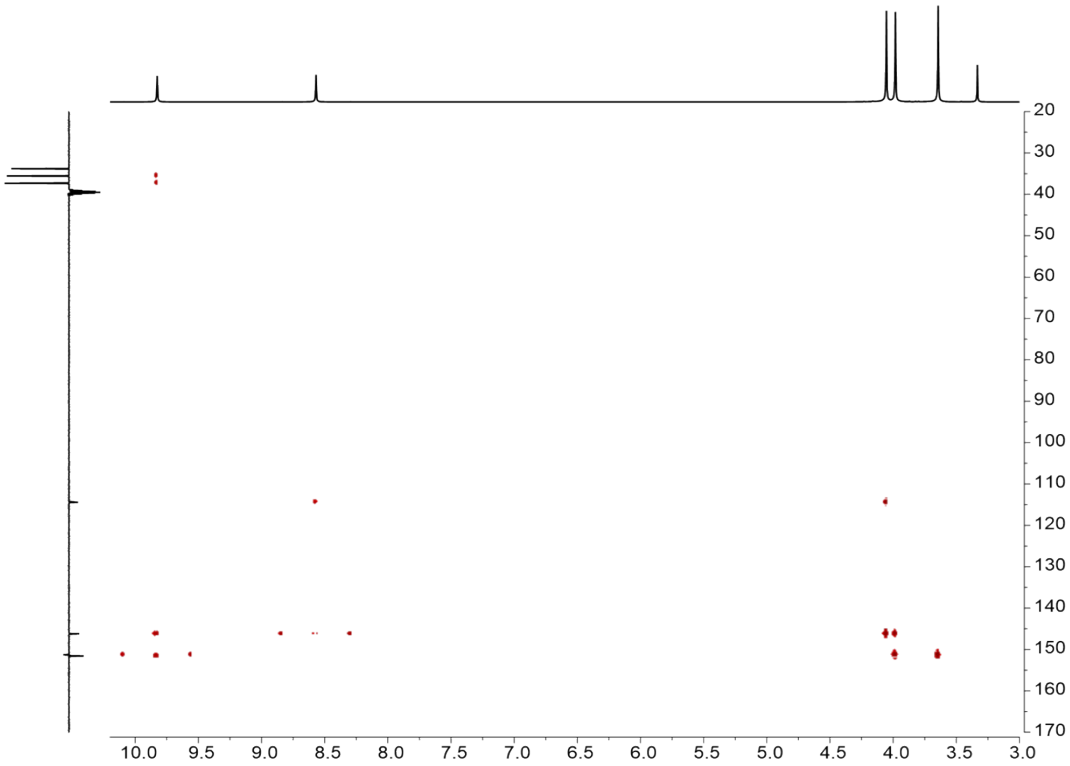

Figure SI-19. ^{1}H-^{13}C HMBC NMR spectrum of **2**[NO_3] in DMSO-d_6 at 298 K.

NMR spectra of 1[Cl]

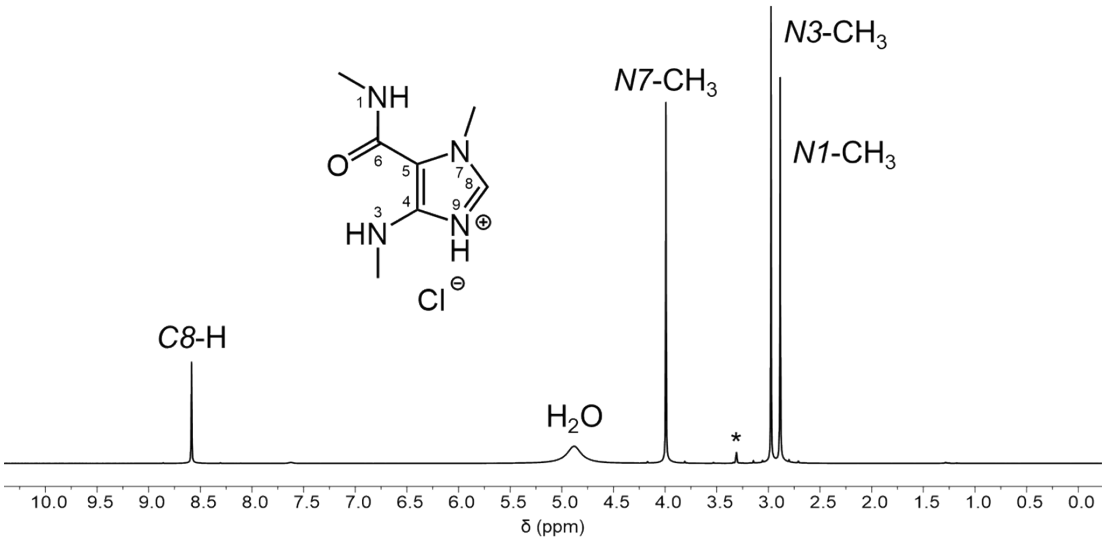

Figure SI-20. ^{1}H NMR spectrum of **1**[Cl] in CD_3OD at 298 K.

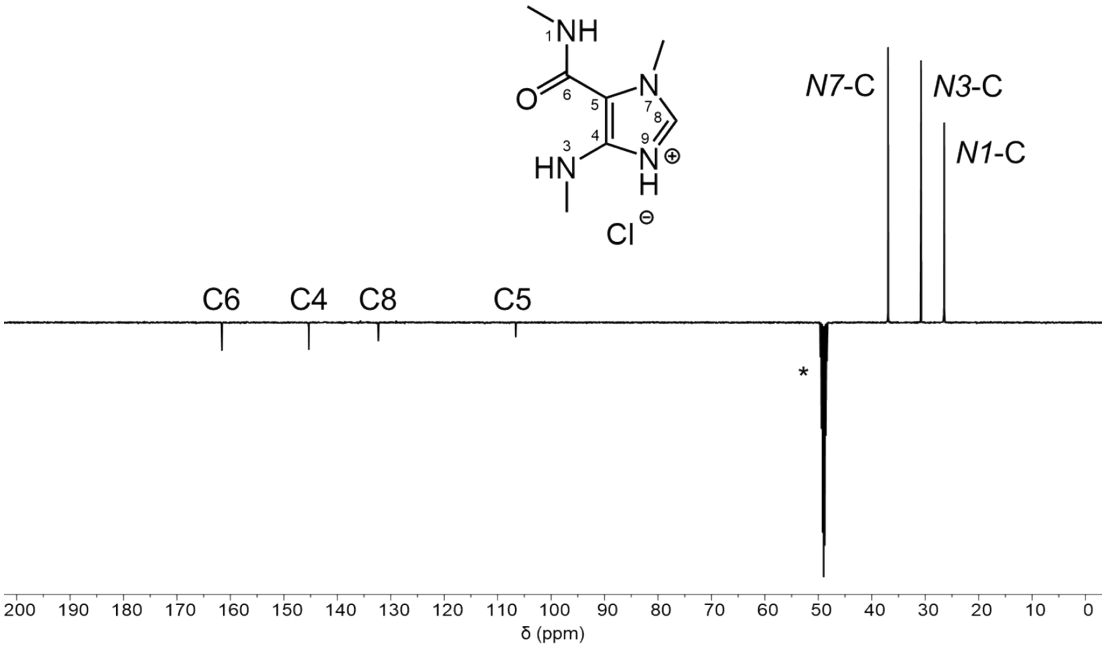

Figure SI-21. $^{13}C\{^{1}H\}$-APT NMR spectrum of **1**[Cl] in CD_3OD at 298 K.

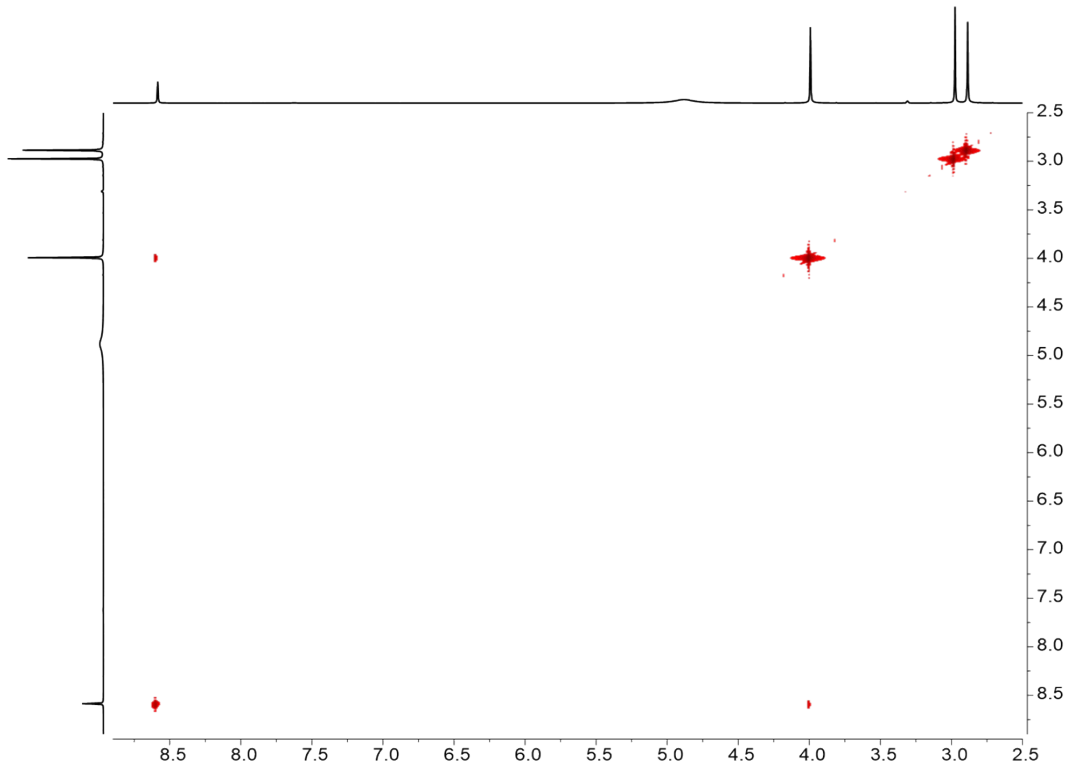

Figure SI-22. ^{1}H-^{1}H COSY NMR spectrum of **1**[Cl] in CD_3OD at 298 K.

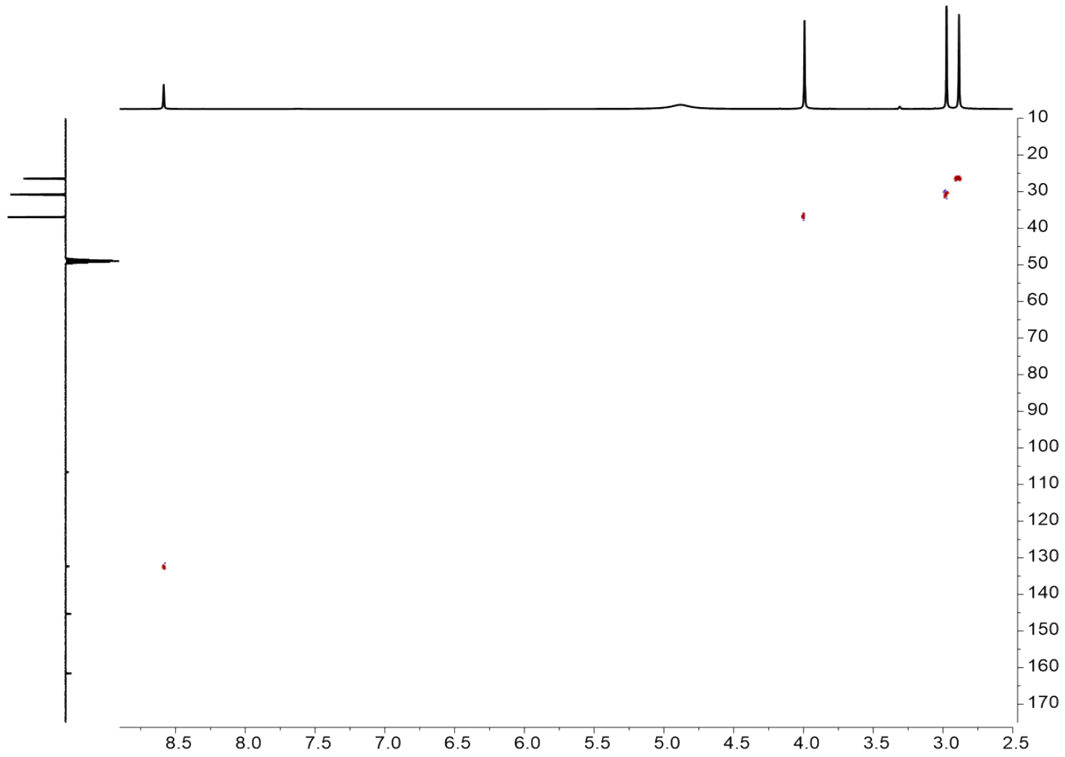

Figure SI-23. ^{1}H-^{13}C HSQC NMR spectrum of **1**[Cl] in CD_3OD at 298 K.

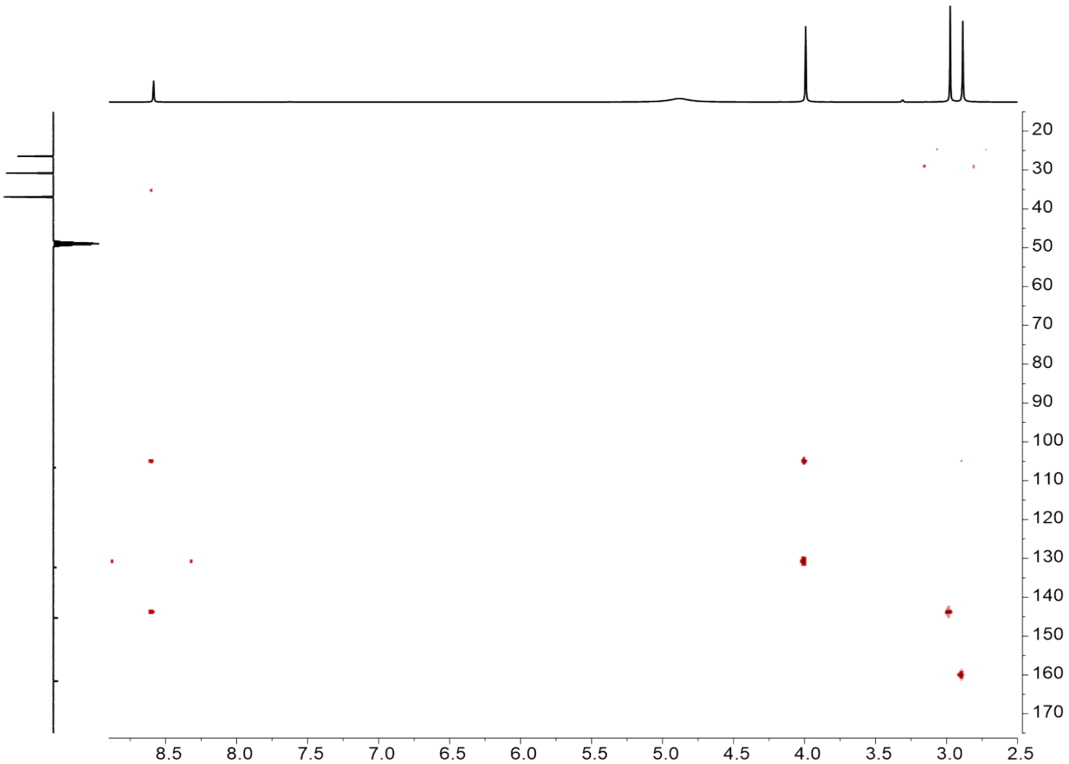

Figure SI-24. ^{1}H-^{13}C HMBC NMR spectrum of **1**[Cl] in CD_3OD at 298 K.

NMR spectra of 2[Cl]

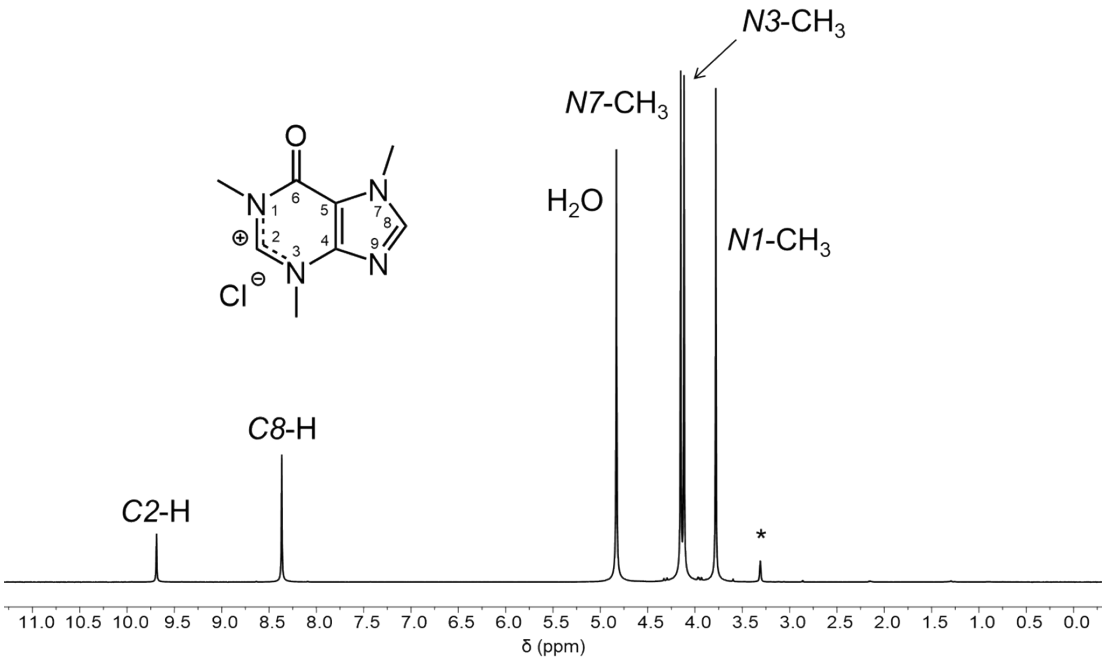

Figure SI-25. ^{1}H NMR spectrum of **2**[Cl] in CD_3OD at 298 K.

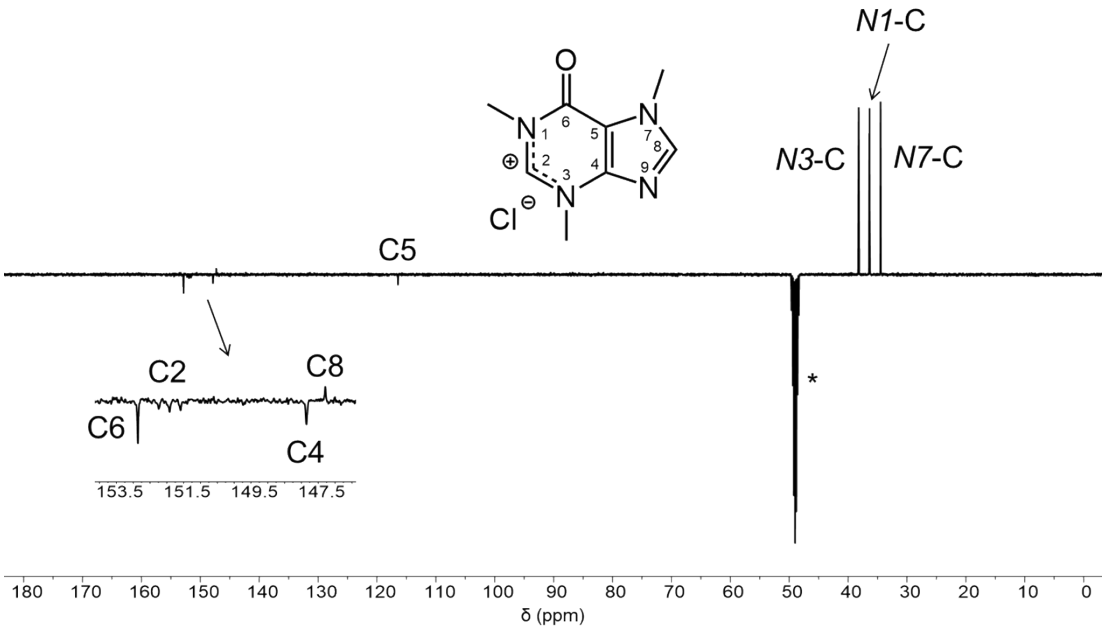

Figure SI-26. $^{13}C\{^{1}H\}$-APT NMR spectrum of **2**[Cl] in CD_3OD at 298 K.

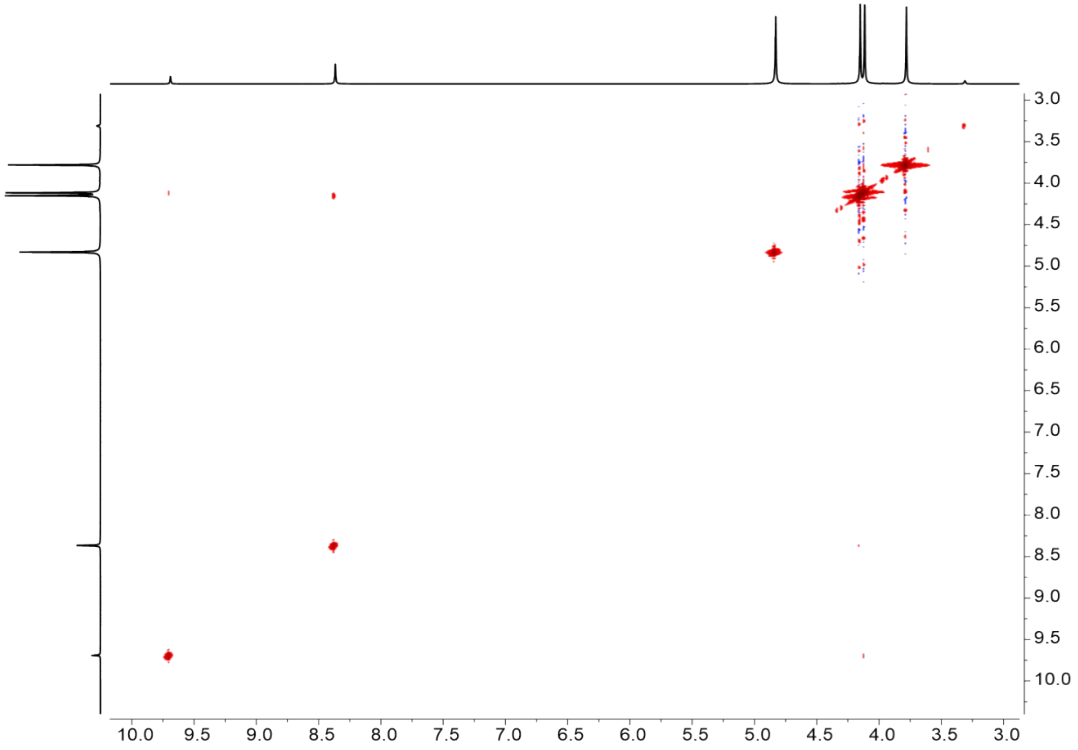

Figure SI-27. ^{1}H-^{1}H COSY NMR spectrum of **2**[Cl] in CD_3OD at 298 K.

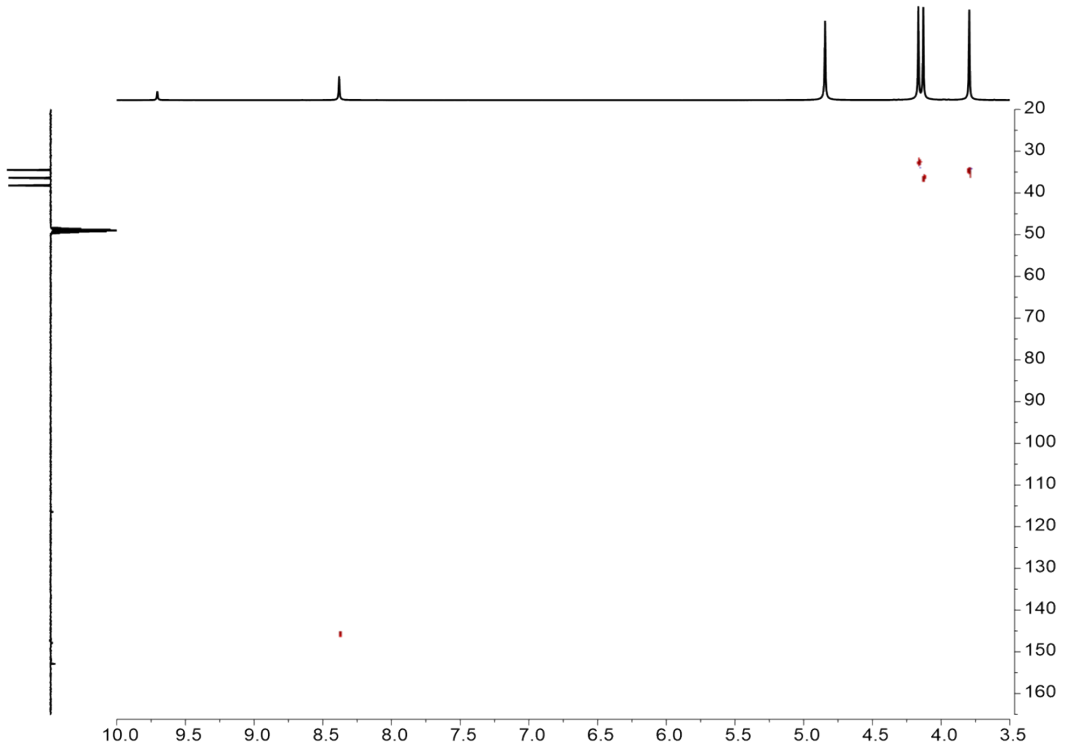

Figure SI-28. ^{1}H-^{13}C HSQC NMR spectrum of **2**[Cl] in CD_3OD at 298 K.

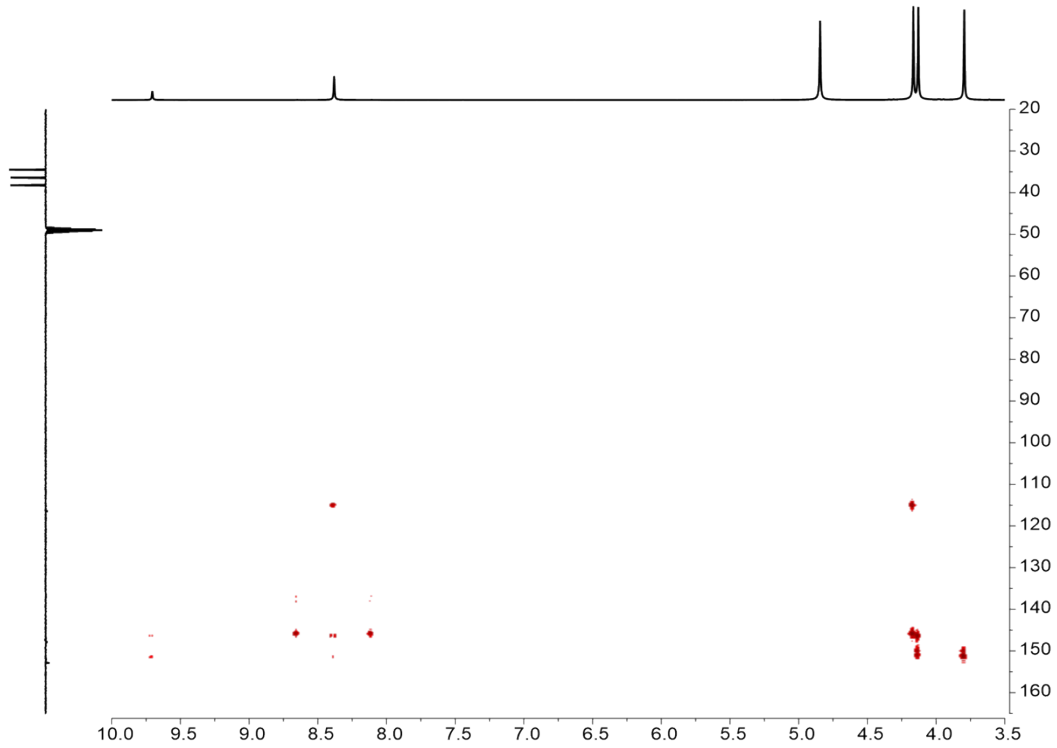

Figure SI-29. ^{1}H-^{13}C HMBC NMR spectrum of **2**[Cl] in CD_3OD at 298 K.

NMR spectra of 2[PF_6]

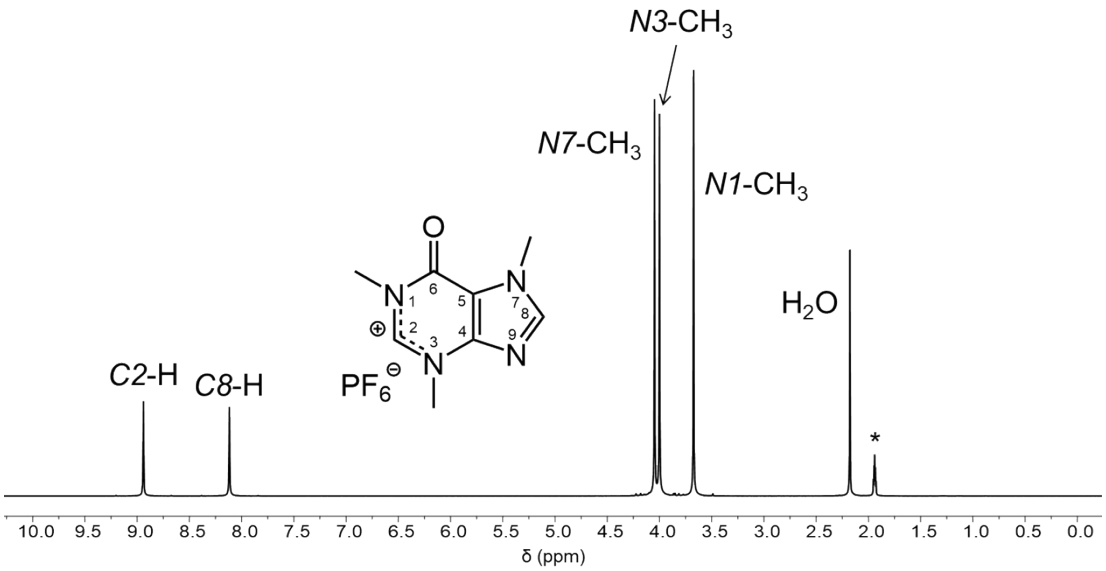

Figure SI-30. ^{1}H NMR spectrum of **2**[PF_6] in CD_3CN at 298 K.

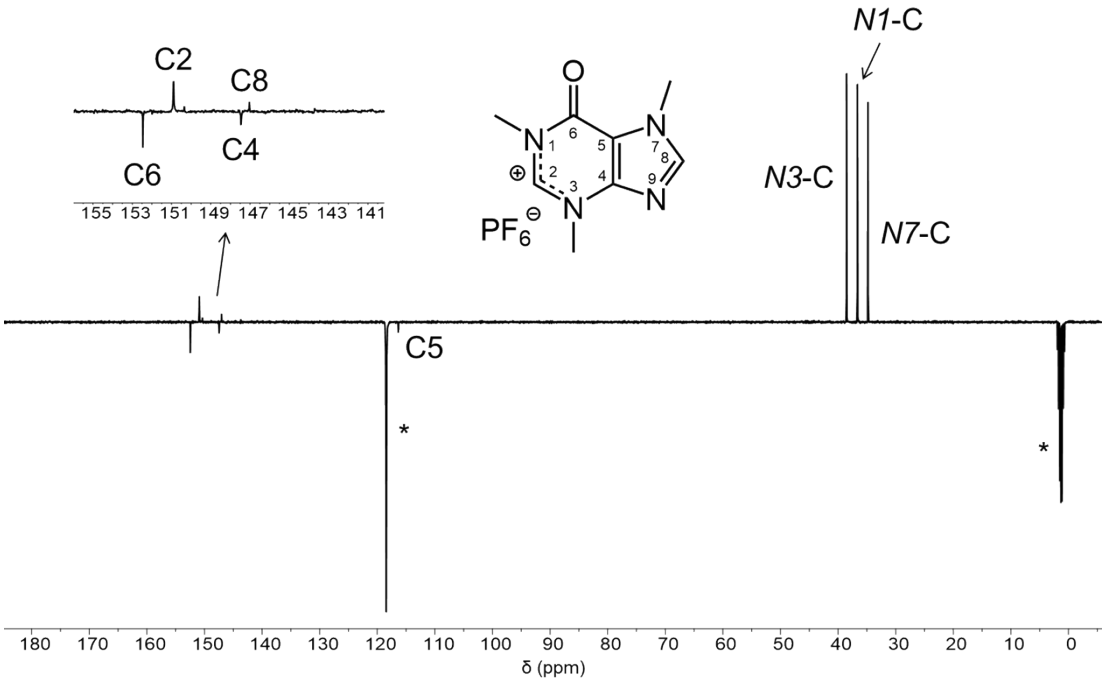

Figure SI-31. $^{13}C\{^{1}H\}$-APT NMR spectrum of **2**[PF_6] in CD_3CN at 298 K.

NMR spectra of 2[Br]

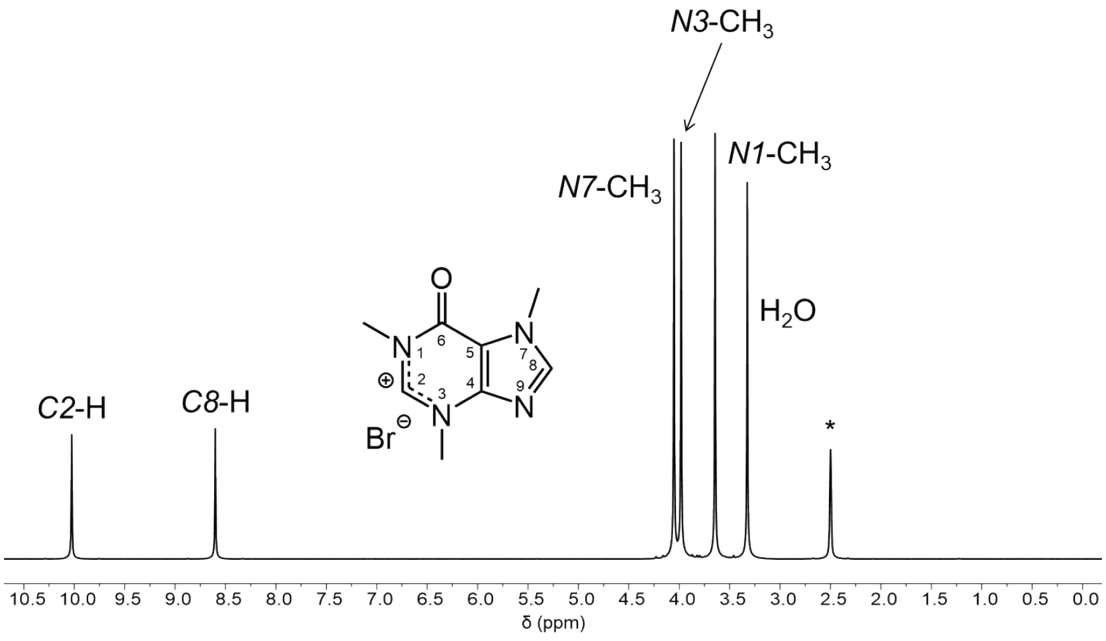

Figure SI-32. ^{1}H NMR spectrum of **2**[Br] in DMSO-d_6 at 298 K.

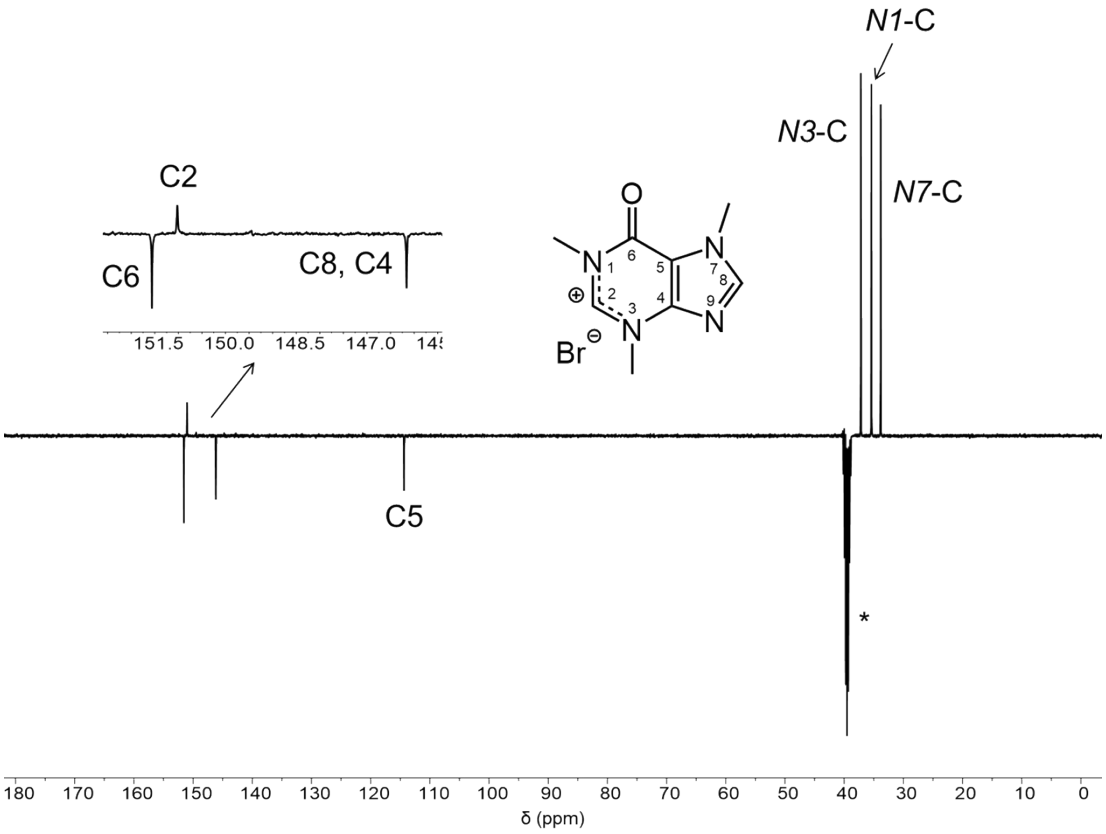

Figure SI-33. $^{13}C\{^{1}H\}$-APT NMR spectrum of **2**[Br] in DMSO-d_6 at 298 K.

NMR spectra of 2[I]

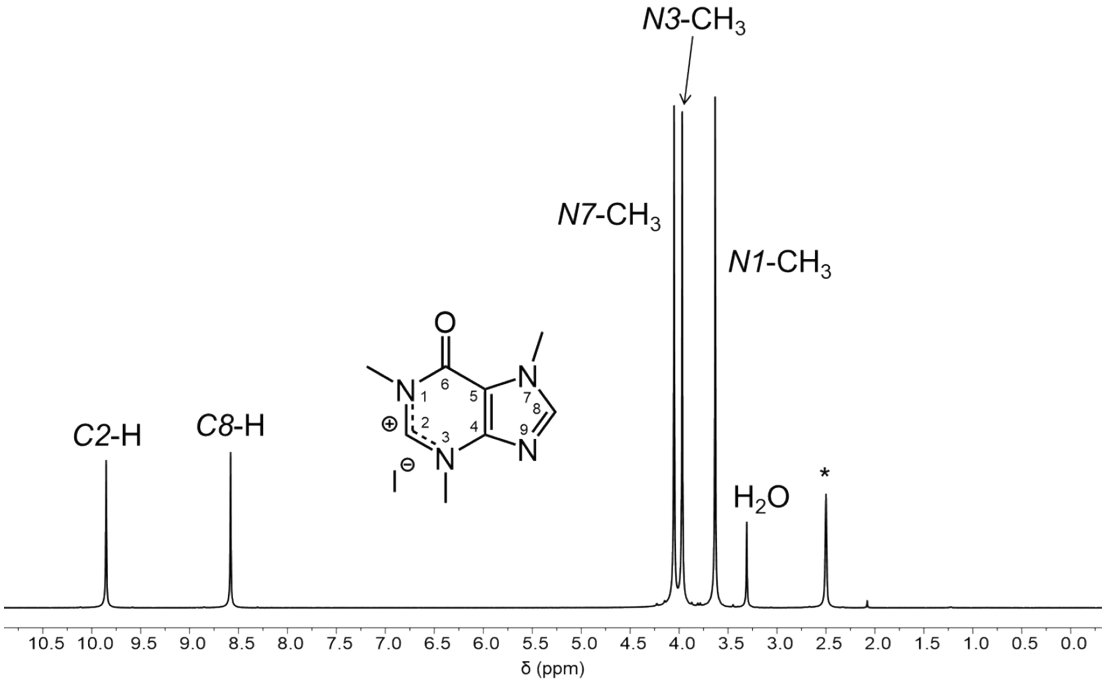

Figure SI-34. ^{1}H NMR spectrum of **2**[I] in DMSO-d_6 at 298 K.

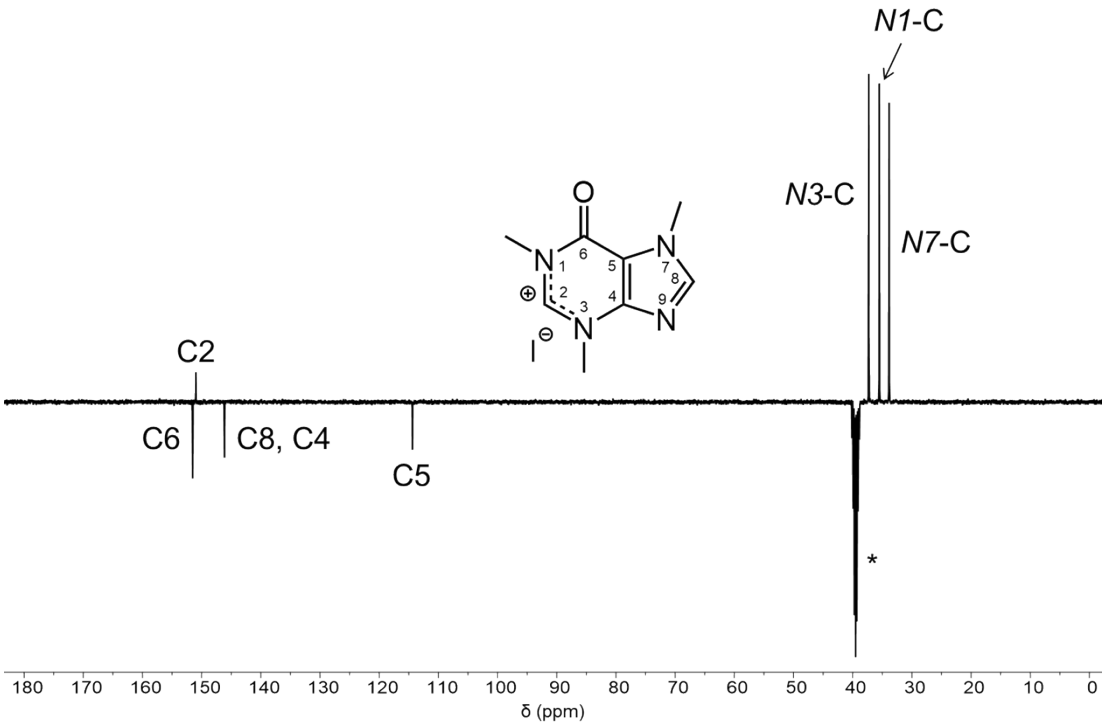

Figure SI-35. $^{13}C\{^{1}H\}$-APT NMR spectrum of **2**[I] in DMSO-d_6 at 298 K.

NMR spectra of 3[Cl]

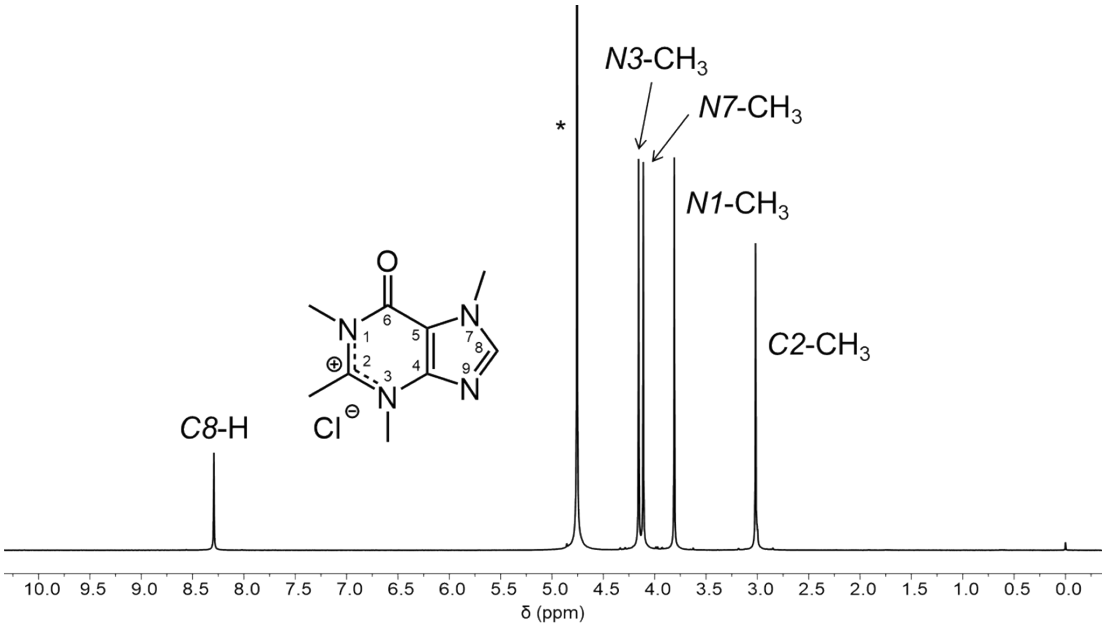

Figure SI-36. ^{1}H NMR spectrum of **3**[Cl] in D_2O at 298 K.

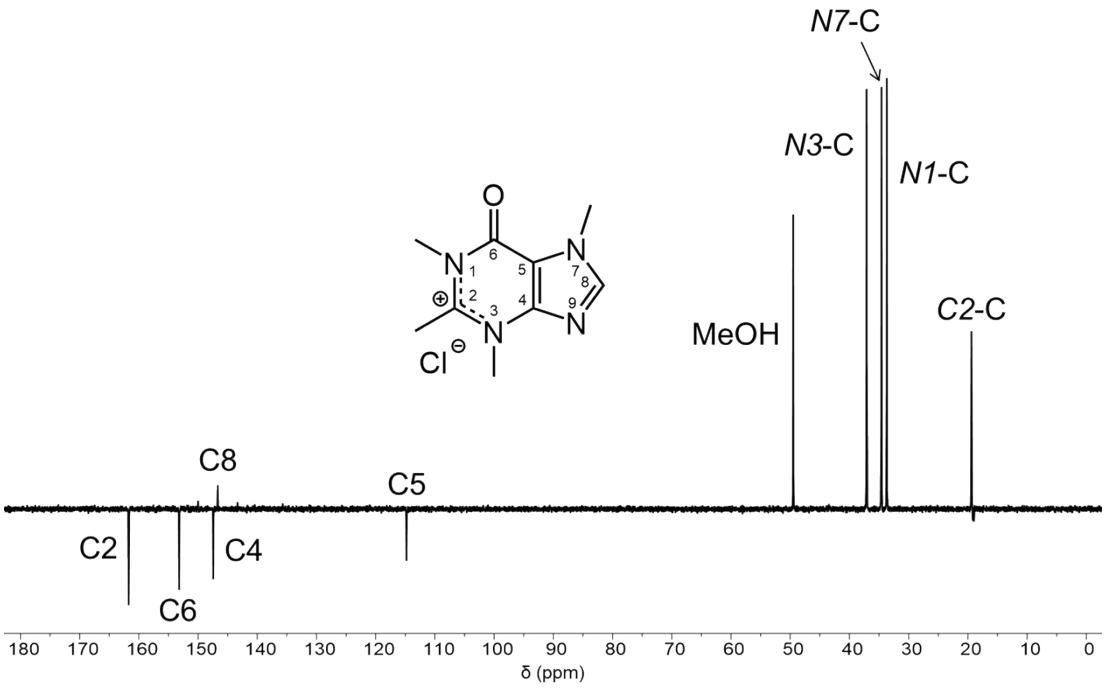

Figure SI-37. $^{13}C\{^{1}H\}$-APT NMR spectrum of **3**[Cl] in D_2O at 298 K.

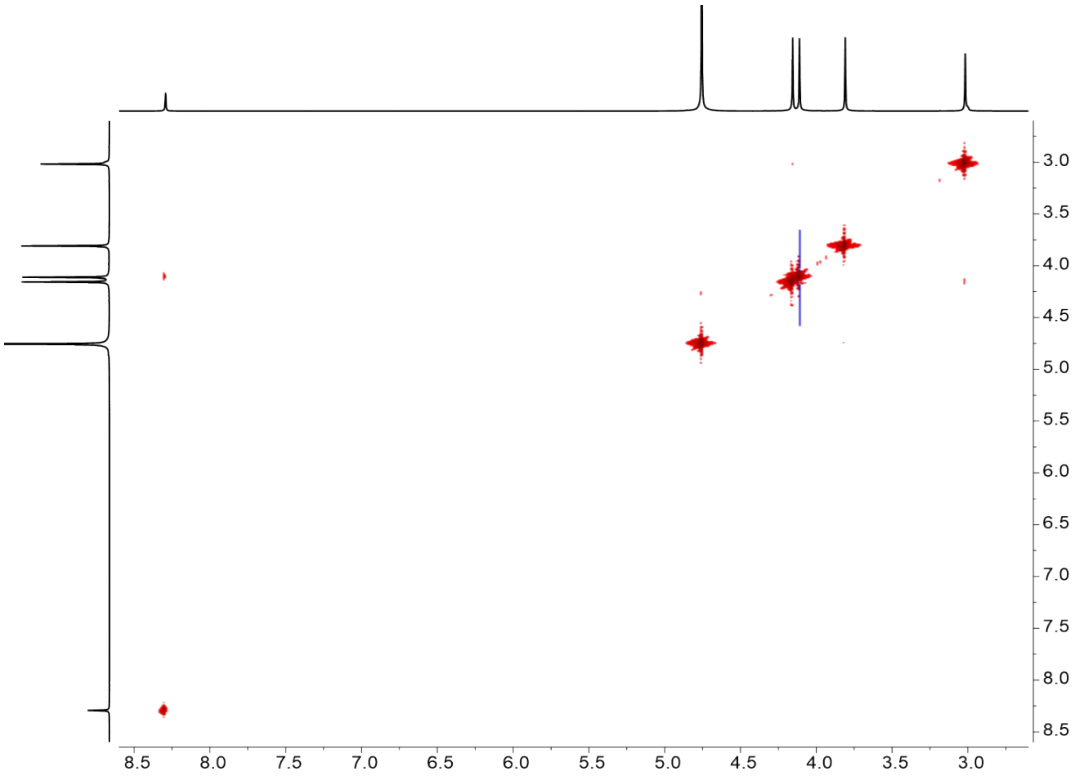

Figure SI-38. ^{1}H-^{1}H COSY NMR spectrum of **3**[Cl] in D_2O at 298 K.

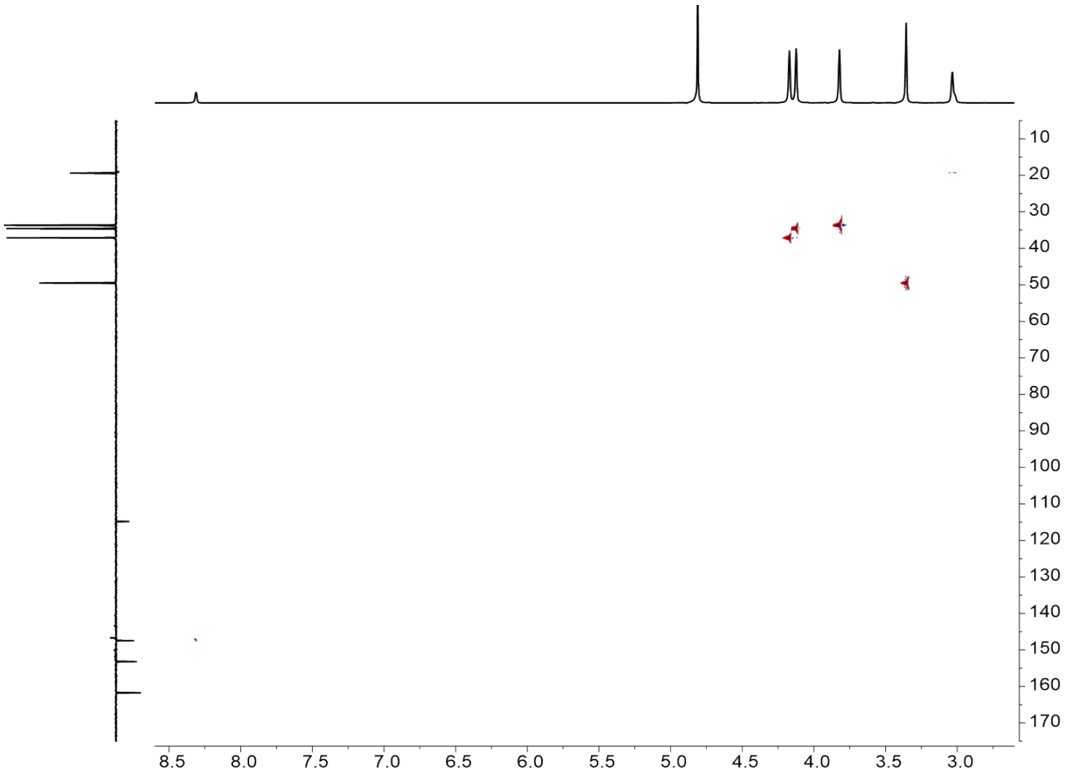

Figure SI-39. ^{1}H-^{13}C HSQC NMR spectrum of **3**[Cl] in D_2O at 298 K.

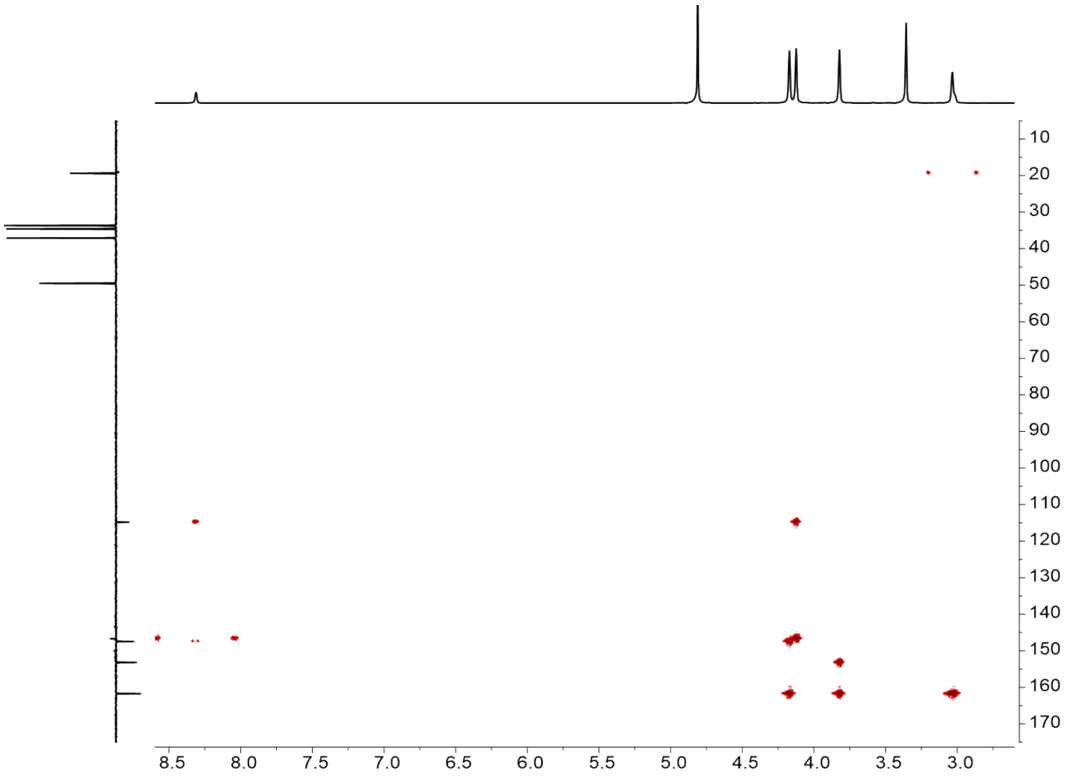

Figure SI-40. ^{1}H-^{13}C HMBC NMR spectrum of **3**[Cl] in D_2O at 298 K.

4. Crystal structure determination

X-ray diffraction data of complexes **1**[NO_3] (CCDC 2475635), **1**[Cl] (CCDC 2475636), **2**[NO_3] (CCDC 2475637), **2**[Cl]·H_2O (CCDC 2475638), **2**[Br]·H_2O (CCDC 2475639), **2**[I] (CCDC 2475640), and **3**[Cl]·$3H_2O$ (CCDC 2475641) were collected on a Bruker D8 Venture diffractometer, with by graphite-monochromated Mo Kα radiation (λ = 0.71073 Å). Single crystals were mounted and coated with perfluoropolyether oil. Diffracted intensities were integrated with SAINT,[SI-3] and corrected of absorption effects was performed with a multi-scan strategy by SADABS.[SI-4, SI-5] All structures were solved by direct methods with the software SHELXS[SI-6] and refined by full-matrix least squares on F^2 with SHELXL program,[SI-7] and the WinGX[SI-8] or Olex2[SI-9] systems. In **2**[Cl]·H_2O, the refined O–H bond lengths are slightly longer than commonly idealized values. As they are supported by electron density maps and remain chemically reasonable, no geometric restraints were applied during refinement. In **3**[Cl]·$3H_2O$, the difference Fourier maps indicate possible minor disorder of the water hydrogen positions. However, this could not be modelled in a stable way, and a simplified model was therefore applied.

Crystal data for compound **1**[NO_3]: $C_7H_{13}N_5O_4$, M_r = 231.22, colorless prisms, triclinic *P–1*, *a* = 6.6071(4) Å, *b* = 7.9107(5) Å, *c* = 10.3623(6) Å, *α* = 110.660(3)°, *β* = 97.406(3)°, *γ* = 90.598(3)°, *V* = 501.63(5) Å^3, *Z* = 2, *T* = 100(2) K, D_{calcd} = 1.531 g cm^{-3}, *μ* = 0.126 mm^{-1}, absorption correction factors min. 0.957 max. 0.969, 11707 reflections, 2780 unique (R_{int} = 0.0174), 2437 observed, R_1 = 0.0375 [I > 2σ(I)], wR_2(F^2) = 0.1074 (all data), GOF = 1.061. CCDC 2475635.

Crystal data for compound **1**[Cl]: $C_7H_{13}ClN_4O$, M_r = 204.66, colorless prism, triclinic *P–1*, *a* = 6.5053(3) Å, *b* = 7.8928(4) Å, *c* = 9.8692(5) Å, *α* = 68.6656(14)°, *β* = 77.5428(14)°, *γ* = 87.0433(15)°, *V* = 460.70(4) Å^3, *Z* = 2, *T* = 100(2) K, D_{calcd} = 1.475 g cm^{-3}, *μ* = 0.381 mm^{-1}, absorption correction factors min. 0.959 max. 0.981, 19802 reflections, 2285 unique (R_{int} = 0.0231), 2261 observed, R_1 = 0.0274 [I > 2σ(I)], wR_2(F^2) = 0.0693 (all data), GOF = 1.086. CCDC 2475636.

Crystal data for compound **2**[NO_3]: $C_8H_{11}N_5O_4$, M_r = 241.22, colorless prisms, monoclinic *P21/c*, *a* = 11.7204(8) Å, *b* = 8.8224(6) Å, *c* = 10.3810(7) Å, *β* = 90.9287(9)°, *V* = 1073.28(13) Å^3, *Z* = 4, *T* = 100(2) K, D_{calcd} = 1.493 g cm^{-3}, *μ* = 0.122 mm^{-1}, absorption correction factors min. 0.880 max. 0.964, 13369 reflections, 2697 unique (R_{int} = 0.0315), 2130 observed, R_1 = 0.0382 [I > 2σ(I)], wR_2(F^2) = 0.0959 (all data), GOF = 1.028. CCDC 2475637.

Crystal data for compound **2**[Cl]·H_2O: $C_8H_{13}ClN_4O_2$, M_r = 232.67, colorless block, monoclinic *P21/c*, *a* = 11.2219(9) Å, *b* = 14.8838(13) Å, *c* = 6.4028(5) Å, *β* = 102.4031(11)°, *V* = 1044.46(15) Å^3, *Z* = 4, *T* = 100(2) K, D_{calcd} = 1.480 g cm^{-3}, *μ* = 0.353 mm^{-1}, absorption correction factors min. 0.886 max. 0.917, 18651 reflections, 2581 unique (R_{int} = 0.0233), 2339 observed, R_1 = 0.0311 [I > 2σ(I)], wR_2(F^2) = 0.0868 (all data), GOF = 1.054. CCDC 2475638.

Crystal data for compound **2**[Br]·H_2O: $C_8H_{13}BrN_4O_2$, M_r = 277.13, colorless block, monoclinic *P21/c*, *a* = 11.4500(3) Å, *b* = 15.0573(4) Å, *c* = 6.4762(2) Å, *β* = 103.1158(9)°, *V* = 1087.41(5) Å^3, *Z* = 4, *T* = 100(2) K, D_{calcd} = 1.693 g cm^{-3}, *μ* = 3.768 mm^{-1}, absorption correction factors min. 0.313 max. 0.547, 26996 reflections, 2689 unique (R_{int} = 0.0432), 2643 observed, R_1 = 0.0198 [I > 2σ(I)], wR_2(F^2) = 0.0530 (all data), GOF = 1.083. CCDC 2475639.

Crystal data for compound **2**[I]: $C_8H_{11}IN_4O$, M_r = 306.11, colorless blocks, orthorhombic *Pca21*, *a* = 11.3493(7) Å, *b* = 11.5417(7) Å, *c* = 8.4397(5) Å, *V* = 1105.52(12) Å^3, *Z* = 4, *T* = 100(2) K, D_{calcd} = 1.839 g cm^{-3}, μ = 2.873 mm^{-1}, absorption correction factors min. 0.663 max. 0.795, 52792 reflections, 2745 unique (R_{int} = 0.0294), 2742 observed, R_1 = 0.0110 [I > 2σ(I)], wR_2(F^2) = 0.0271 (all data), GOF = 1.069. CCDC 2475640.

Crystal data for compound **3**[Cl]·3H_2O: $C_9H_{19}ClN_4O_4$, M_r = 282.73, colorless blocks, monoclinic *P21/n*, *a* = 13.5822(5) Å, *b* = 6.6192(2) Å, *c* = 16.0458(7) Å, *β* = 109.3822(15)°, *V* = 1360.81(9) Å^3, *Z* = 4, *T* = 100(2) K, D_{calcd} = 1.380 g cm^{-3}, μ = 0.294mm^{-1}, absorption correction factors min. 0.952 max. 0.985, 38366 reflections, 3381 unique (R_{int} = 0.0596), 2928 observed, R_1 = 0.0432 [I > 2σ(I)], wR_2(F^2) = 0.1301 (all data), GOF = 1.044. CCDC 2475641.

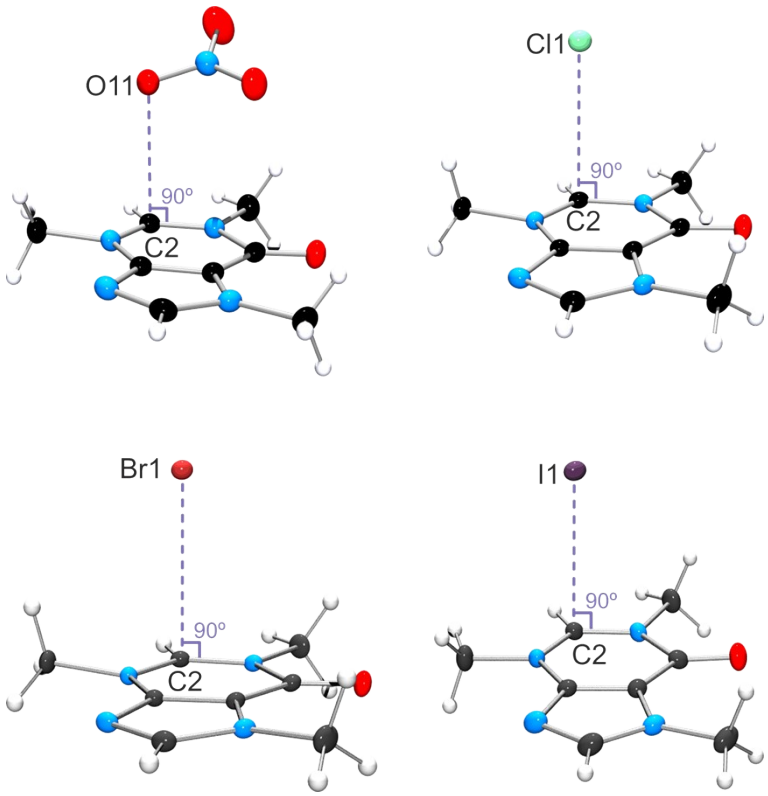

Figure SI-41. View of n⟶π* interactions in **2**[Cl]·H_2O and **2**[NO_3].

5. Hydrogen Bonding

Table SI-1. Geometrical parameters [Å, °] of hydrogen bonds.

Compound	H bonds	H···A	D···A	D–H···A
Cation···Water				
2[Cl]·H_2O	O1w–H···Cl	2.16(4)	3.2646(12)	165(3)
		2.22(3)	3.2702(14)	156(2)
2[Br]·H_2O	O1w–H···Br	2.40(3)	3.4011(12)	171(2)
		2.42(3)	3.4054(12)	161(3)
3[Cl]·3H_2O	O1w–H···Cl	2.2176(5)	3.0747(16)	175.58(9)
		2.2236(4)	3.0893(15)	174.46(11)
Cation···Anion				
2[Cl]·H_2O	C2–H2···Cl	2.519(18)	3.4122(13)	168.2(14)
2[Cl]·H_2O	C8–H8···Cl	2.650(17)	3.5784(14)	178.5(14)
2[Br]·H_2O	C2–H2···Br	2.615(3)	3.5475(13)	167.16(7)
2[Br]·H_2O	C8–H8···Br	2.745(3)	3.6906(13)	174.04(8)
2[I]	C2–H2···I	2.8136(3)	3.7312(18)	162.48(11)
2[I]	C8–H8···I	2.9909(3)	3.859(2)	152.54(13)
3[Cl]·3H_2O	C8–H8···Cl	2.7291(5)	3.5671(19)	147.48(11)

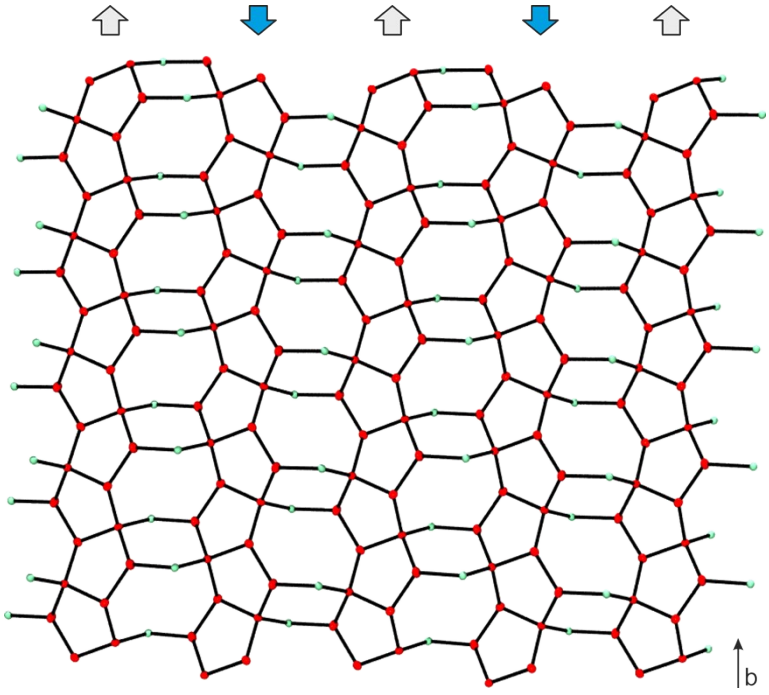

Figure SI-42. Hydrogen bonding pattern in **3**[Cl]·3H_2O. Red: O atoms. Green: Cl^- anions.

6. Computational details

DFT electronic structure calculations were carried out with Gaussian16 using the M06-2X functional and the all-electron jorge-TZP basis set for all atoms. Interaction energies were calculated by means of the supermolecule approach and corrected for the BSSE with the Counterpoise method. NBO/NPA analyses were performed with the NBO3.1 module included in Gaussian16 and the corresponding orbitals represented with IQMol 2.15.0 (s = 0.05 $Å^{-3}$). We used AIMAll for the topological analysis of the electron density within the QTAIM framework. MEP maps were built on the corresponding 0.001 au isosurfaces with GaussView. Interatomic distances are given throughout the article as penetration indexes. The penetration index p_{AB} indicates the degree of interpenetration of the van der Waals crusts of atoms A and B, from 0% (canonical vdW contact) to 100% (canonical bond distance) and is defined as $p_{AB} = 100(v_A + v_B - d_{AB})/(v_A + v_B - r_A + r_B)$ where '*v*' is the van der Waals radius and '*r*' the covalent radius of a given atom. For computing *p* we used standard sets of van der Waals[SI-10] and covalent[SI-11] radii. Further details on the use of penetration indexes and their applications can be found in a recent publication.[SI-12]

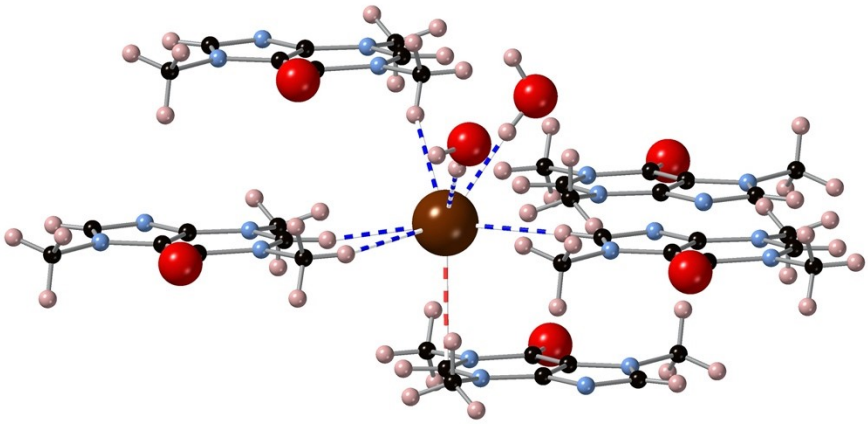

Figure SI-43. Short contacts between bromide and the surrounding atoms in **2**[Br]·H_2O.

7. Hirshfeld surface and fingerprint plot analysis

Hirshfeld surfaces and fingerprint plots of **2**[Cl]·H_2O and **2**[Br]·H_2O were generated and analyzed using *Crystal Explorer*.[SI-13] As stated in the main text, fingerprint plots display similar features: Figure 2 for **2**[Br]·H_2O and Figure SI-42 for **2**[Cl]·H_2O.

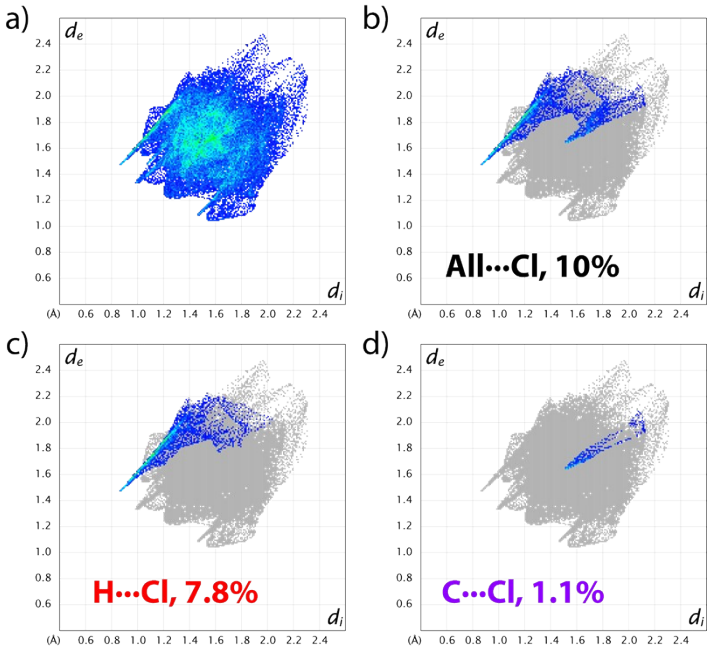

Figure SI-44. Fingerprint plot for cation **2** in **2**[Cl]·H_2O. a) All contacts; b) Contacts involving Cl as outside atom; c) H···Cl contacts; d) C···Cl contacts.

8. Quantum crystallography

Data collection strategy. Diffraction images were collected with a fixed sample-detector distance (42 mm) using narrow frames (0.3° ω or ϕ rotation) at different detector positions (2θ = 46.93°, 64.70°) in order to assure a perfect coverage of all independent reflections. The exposure time was adapted for each position (7, 20 s, respectively). Integration of diffraction images were performed enables least square profile fitting, and using recurrence background and a flexible integration box size. Analysis of the reflection data is summarized in Table SI-2.

Table SI-2. Analysis of reflection data: number of reflections collected (#data) and theoretical (#theo), completeness (%Comp), redundancy (red), mean intensity (<I>), mean Intensity over sigma (<I/σ>), statistical agreement factors R_{merge} and R_{sigma}.

Resolution	#Data	#Theo	%Comp	Red	$< I >$	$< I/\sigma >$	R_{merge}	R_{sigma}
Inf- 1.75	235	237	99.20	11.92	62.41	59.77	0.0340	0.0206
1.75 - 1.15	566	566	100.00	23.11	30.08	88.49	0.0327	0.0178
1.15 - 0.91	774	774	100.00	28.27	17.06	95.93	0.0276	0.0111
0.91 - 0.79	825	825	100.00	28.76	9.22	87.23	0.0303	0.0086
0.79 - 0.72	749	749	100.00	27.00	6.16	76.35	0.0362	0.0096
0.72 - 0.67	783	783	100.00	25.97	4.78	66.68	0.0412	0.0106
0.67 - 0.63	764	764	100.00	25.47	3.44	57.28	0.0497	0.0123
0.63 - 0.59	1015	1015	100.00	24.39	2.53	48.60	0.0589	0.0149
0.59 - 0.57	636	636	100.00	22.42	1.78	37.01	0.0757	0.0199
0.57 - 0.55	696	696	100.00	21.44	1.61	34.70	0.0858	0.0221
0.55 - 0.53	817	817	100.00	21.03	1.27	29.48	0.1009	0.0265
0.53 - 0.51	959	959	100.00	20.68	0.95	24.13	0.1208	0.0335
0.51 - 0.49	1099	1099	100.00	19.22	0.74	19.68	0.1479	0.0429
0.49 - 0.48	645	645	100.00	17.46	0.61	16.18	0.1786	0.0546
0.48 - 0.47	678	678	100.00	15.03	0.53	13.37	0.2006	0.0674
0.47 - 0.46	732	732	100.00	14.00	0.45	12.42	0.1973	0.0720
0.46 - 0.45	824	824	100.00	12.79	0.38	10.57	0.2208	0.0866
0.45 - 0.44	873	873	100.00	11.79	0.33	9.06	0.2507	0.1028
0.44 - 0.43	965	965	100.00	9.30	0.30	6.93	0.2834	0.1342
0.43 - 0.42	1001	1004	92.70	5.43	0.23	4.19	0.3161	0.2475
0.52 - 0.42	7304	7382	98.90	13.35	0.48	12.29	0.1795	0.0779
Inf- 0.42	15629	15709	99.50	19.16	4.69	37.47	0.0437	0.0182

Experimental electron density model: An additional data set of **2**[Br]·H_2O was recorded until high resolution. Refinement of the high-quality data allowed to determine a partial occupancy factor for the water molecule. The structural model of **2**[Br]·H_2O obtained with Olex2[SI-9] was imported as initial model to MoPro software.[SI-14]

Independent atom model was refined by full-matric least square refinement of scale factor using a I>3σ(I) threshold as follow: i) scale factor at whole resolution, ii) coordinates and anisotropic displacement parameters of non-H atoms (excluding water) with high order resolution data ($\sin\theta/\lambda > 0.8$ Å^{-1}). Hydrogen atoms have been included in the model in calculated positions. The anisotropic displacement of hydrogen atoms (excluding those of water) have been constrained to the values obtained with SHADE3 server.[SI-15] Anharmonic thermal motion description up to fourth order of Gram-Charlier expansion was used for bromine atom, as the achieved resolution is close to the required value (0.42 Å) following Kuhn's rule.[SI-16] At the end of the IAM refinement,

the scale factor was refined using all the data set resolution in order to calculate dynamic deformation charge density maps (Figure SI-51).

Asphericity of the electron density distribution of **2**[Br]·H_2O has been considered with a multipolar refinement using Hansen-Coppens formalism:[SI-17]

$$\rho(\vec{r}) = \rho_{core}(r) + P_{val}(\kappa.r) + \sum_{l=0}^{l_{max}} \kappa'^{3} R_{n_l}(\kappa' \cdot r) \sum_{m=0}^{l} P_{lm} y_{lm\pm}(\theta,\varphi)$$

Where the two first terms correspond to spherical core and valence density, and the third term represents the aspherical part of the valence density (defined with the atomic local axes detailed in Table SI-3).

The charge density of **2**[Br]·H2O was refined against F^2 with *MoPro* program,[SI-13] using all the resolution. Multipoles were restrained to dipole level for H atoms, octupolar level for C, N and O, and hexadecapolar level for bromine atom. Multipolar parameters were refined in successive steps. Chemical and symmetry restrains (Table SI-4) were used in the initial steps of the refinement and subsequently released. The expansion/contraction parameters (κ and κ') of hydrogen atoms were restrained to the 1.16(2) value. κ' parameters of hydrogen atoms of water molecule were kept fixed with a 1.16 value.

Multipolar refinement was carried out in systematic steps, refining scale factor, valence population (P_{val}), multipole population P_{lm}; and expansion/contraction factors κ , refined together with positions and atomic displacement parameters; expansion/contraction factors κ' were refined separately. First steps of the refinement were performed using symmetry restraints and reflections with I/σ >3. Once all the parameters have converged, reflections with I/σ >0 were used and restraints were released.

Final residual density maps are depicted in Figure SI-47. Highest residues are observed close to bromine atom core. Refinement details are reported in Table SI-5.

Table SI-3. Atomic local axis system.

Atom	Axis definition	Atom	Axis definition
Br1	bZX C2 O1W	H31, H32, H33	ZX C3 N3
N1	bXY C6 C2	C4	bXY N3 N9
N3	bXY C4 C2	C5	bXY C6 C4
N7	bXY C8 C5	C6	bXY O6 N1
N9	bXY C4 C8	C7	ZX N7 H73
O6	XY C6 N1	H71, H72, H73	ZX C7 N7
C1	ZX N1 H12	C8	bXY N7 N9
H11, H12, H13	ZX C1 N1	H8	ZX C8 N7
C2	bXY N3 N1	O1W	bZX Br1 C3
H2	ZX C2 N3	H1W	ZX O1W C3
C3	ZX N3 H31	H2W	ZX O1W Br1

Table SI-4. Local restraints used in initial steps of the refinement.

Geometrical restraints (kept throughout the entire refinement)

```
DISTAN  C1  1  H11  1  1.095  0.005
DISTAN  C1  1  H12  1  1.095  0.005
DISTAN  C1  1  H13  1  1.095  0.005
DISTAN  C2  1  H2   1  1.083  0.005
DISTAN  C3  1  H33  1  1.095  0.005
DISTAN  C3  1  H32  1  1.095  0.005
DISTAN  C3  1  H31  1  1.095  0.005
DISTAN  C7  1  H72  1  1.095  0.005
DISTAN  C7  1  H73  1  1.095  0.005
DISTAN  C7  1  H71  1  1.095  0.005
DISTAN  C8  1  H8   1  1.083  0.005
DISTAN  O1W 1  H2W  1  0.983 0.005
DISTAN  O1W 1  H1W  1  0.983 0.005
SIMDIS 1 C1 H11 C1 H12 C1 H13 0.005
SIMDIS 1 N1 H11 N1 H12 N1 H13 0.005
SIMDIS 1 H11 H12 H11 H13 H12 H13 0.005
SIMDIS 1 N3 H2 N1 H2 0.005
SIMDIS 1 C3 H33 C3 H32 C3 H31 0.005
SIMDIS 1 N3 H33 N3 H32 N3 H31 0.005
SIMDIS 1 H33 H32 H33 H31 H32 H31 0.005
SIMDIS 1 C7 H72 C7 H73 C7 H71 0.005
SIMDIS 1 N7 H72 N7 H73 N7 H71 0.005
SIMDIS 1 H72 H73 H72 H71 H73 H71 0.005
SIMDIS 1 N7 H8 N9 H8 0.005
SIMDIS 1 O1W H2W O1W H1W 0.005
```

Local symmetry restraints

```
RSYMUL mz   N1   1  0.01
RSYMUL mz   N3   1  0.01
RSYMUL mz   O6   1  0.01
RSYMUL mz   C4   1  0.01
RSYMUL mz   C5   1  0.01
RSYMUL mz   C6   1  0.01
RSYMUL mymz N7   1  0.01
RSYMUL mymz N9   1  0.01
RSYMUL mymz C2   1  0.01
RSYMUL mymz C8   1  0.01
RSYMUL 3m   C1   1  0.01
RSYMUL 3m   C3   1  0.01
RSYMUL 3m   C7   1  0.01
```

Similarity restraints

```
SIMPVM  1  C1  C3  C7  0.01
SIMKAP  1  C1  C3  C7  0.01
SIMPVM  1  H11  H12  H13  H31  H32  H33  H71  0.01
SIMPVM  1  H11  H12  H13  H31  H32  H33  H71  H72  H73  0.01
SIMPVM  1  H2  H8  0.01
SIMPVM  1  H1W  H2W  0.01
```

Restraints in H atoms kappa values (kept throughout the entire refinement)

```
RESKP1  H11  1  1.16  0.01
RESKP2  H11  1  1.16  0.01
RESKP1  H2  1  1.16  0.01
RESKP2  H2  1  1.16  0.01
RESKP1  H1W  WAT  1.16  0.01
RESKP2  H1W  WAT  1.16  0.01
SIMKAP   1  H11 H12 H13 H31 H32 H33 H71 H72 H73  0.01
SIMKAP   1  H2 H8  0.01
SIMKAP   1  H1W H2W  0.01
```

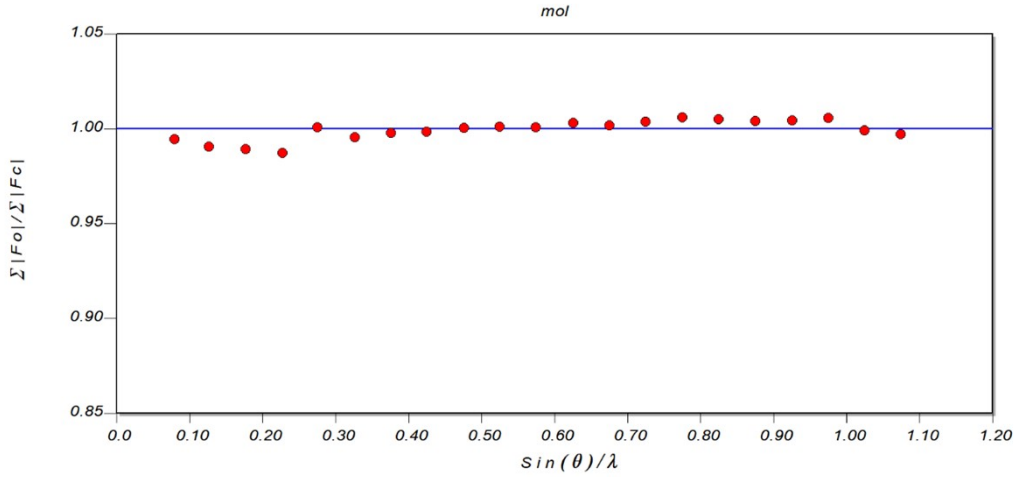

Figure SI-45. XDRK plot showing the fit of $\sum(F_o^2)/\sum(F_c^2)$ *as a function of resolution.*

Note: Figures SI-46 and SI-47 depict the residual density maps, after the independent atom refinement (IAM) and multipolar refinement respectively, calculated on the same reflection dataset.

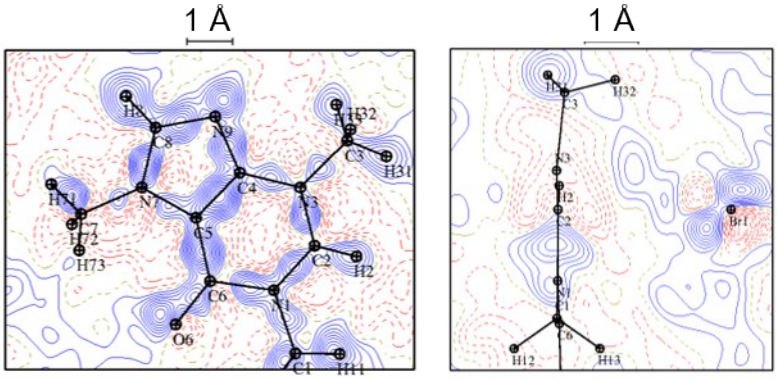

Figure SI-46. Residual density maps of **2**[Br]·H_2O after *IAM* refinement, at contour level of 0.05 e $Å^{-3}$, with sinθ/λ < 0.70 $Å^{-1}$. Mean planes defined by N7–N3–N1 and C2–Br1–N1 atoms, respectively.

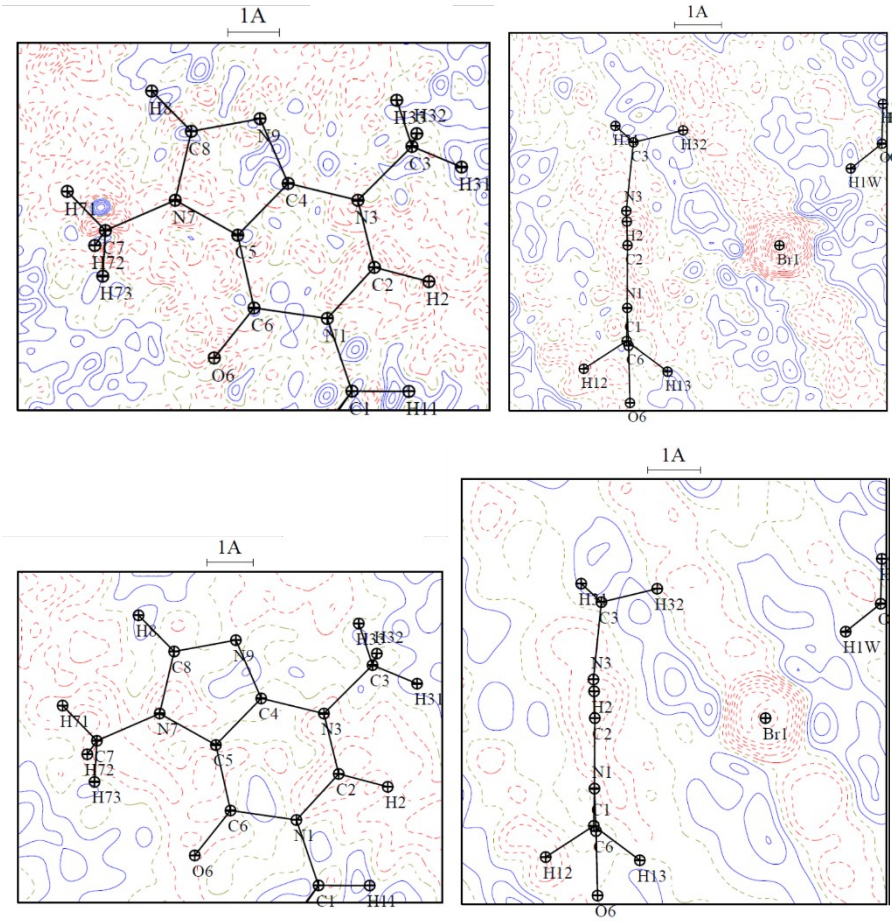

Figure SI-47. Residual density maps of **2**[Br]·H_2O after multipolar refinement, at contour level of 0.05 e Å^{-3}, with all resolution (up) and with sinθ/λ > 0.70 Å^{-1} (down) Mean planes defined by N7–N3–N1 and C2–Br1–N1 atoms, respectively.

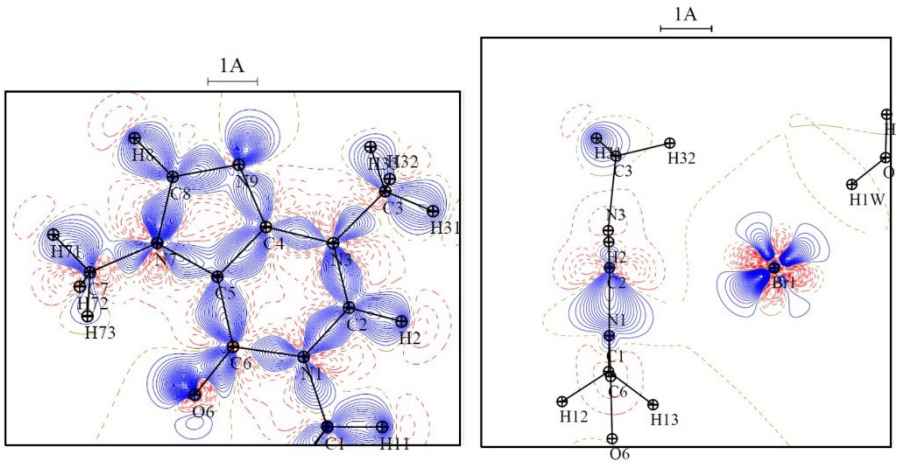

Figure SI-48. Static deformation maps of **2**[Br]·H_2O after multipolar refinement, at contour level of 0.05 e Å^{-3}. Mean planes defined by N7–N3–N1 and C2–Br1–N1 atoms, respectively.

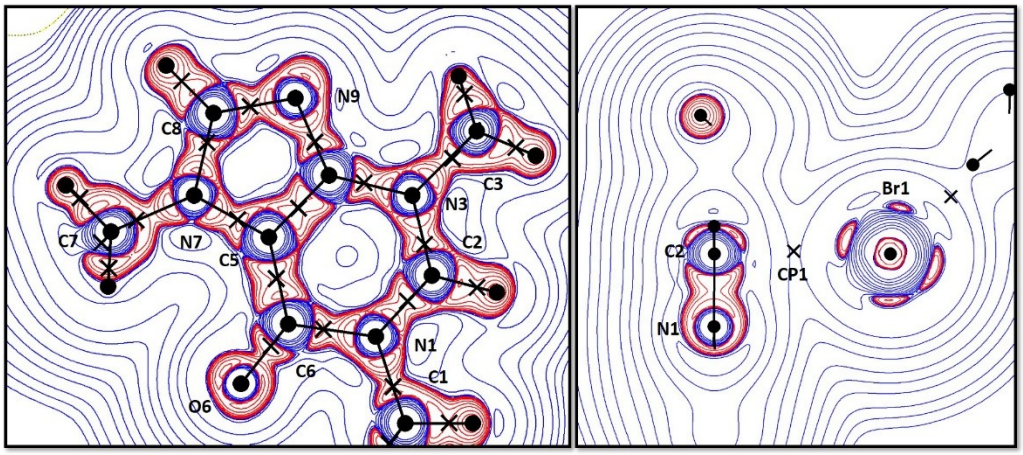

Figure SI-49. Laplacian maps of **2**[Br]·H_2O after multipolar refinement. Logarithmic scale. Intra- and intermolecular CP are depicted as cross in left and right figures, respectively.

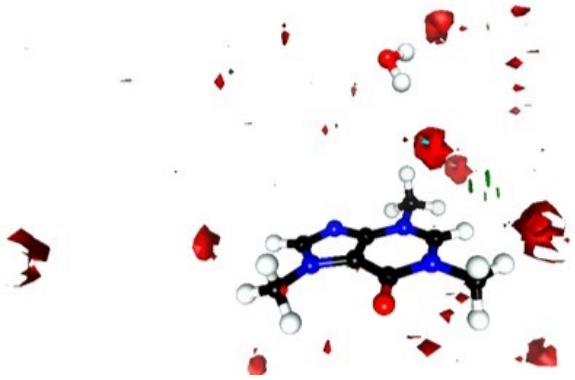

Figure SI-50. Residual density map, with isocontour ±0.24 e/Å^3*. Positive and negative contours are plotted in green and red, respectively.*

Table SI-4. Crystallographic refinement details of **2**[Br]·H_2O from high resolution data.

Crystal data	CCDC 2475642.	
Chemical Formula	$C_8H_{11}N_4O$, Br·0.804(H_2O)	
M_r	273.62	
Crystal system, space group	Monoclinic, $P2_1/c$	
Temperature (K)	100(1)	
a,*b*,*c* (Å)	11.4461(5), 15.0792(7), 6.4594(3)	
β (°)	103.2320(10)	
V (Å^3)	1085.28(9)	
Z	4	
Radiation type	Mo K (λ = 0.71073 Å)	
μ (mm^{-1})	3.773	
Crystal size (mm)	0.110 × 0.120 × 0.158	
Data collection		
Diffractometer	Bruker D8 Venture with PHOTON III detector	
Absorption correction	Multi-scan	
T_{min}, T_{max}	0.6437 / 0.7503	
number of measured / independent reflections (mean redundancy)	276116 / 12173 (22.7)	
R_{int}	0.0437	
$(\sin\theta/\lambda)_{max}$ (Å^{-1})	1.19 [*d*= 0.42 Å]	
Completeness to $(\sin\theta/\lambda)_{max}$	99.9 % (5 missing reflections)	
Refinement	**IAM**	**Multipolar**
Refinement based on	F^2	F^2
R [F^2>2σ(F^2)], wR(F^2), GooF	0.0219, 0.0622, 1.065	0.0216, 0.0329, 1.02
Number of parameters	148	505
Δρ (e Å^{-3})	–1.22 / 1.07	–0.48 / 0.31

Topological analysis of the covalent bonds

A quantitative analysis of the topological properties at bond critical points of covalent bonds in **2**[Br]·H_2O is summarized in Table SI-3.

Table SI-5. Topological properties of (3,–1) CPs in covalent interactions of **2**[Br]·H_2O: d_{12}: bond path length, d_{1CP} and d_{2CP}: distances from atom 1 and atom 2 (forming the bond) to CP (Å); ρ_{CP} electron density (e Å^{-3}), $\nabla^2\rho_{CP}$, Laplacian (e Å^{-5}), λ_i Hessian eigenvalues (e Å^{-5}) and ε ellipticity.

Bond	d_{12}	d_{1CP}	d_{2CP}	ρ_{CP}	$\nabla^2\rho_{CP}$	λ_1	λ_2	λ_3	ε
N1–C1	1.4692	0.8540	0.6155	1.669	–8.13	–11.25	–10.58	13.69	0.06
N1–C2	1.3314	0.7580	0.5730	2.496	–25.90	–22.50	–18.28	14.87	0.23
N1–C6	1.4188	0.8551	0.5653	1.828	–16.35	–15.20	–11.99	10.84	0.27
N3–C2	1.3212	0.8040	0.5186	2.445	–27.93	–22.30	–16.84	11.24	0.32
N3–C3	1.4689	0.8889	0.5815	1.570	–10.34	–10.52	–9.61	9.78	0.09
N3–C4	1.3749	0.7935	0.5810	2.063	–19.52	–18.27	–14.36	13.11	0.27
N7–C5	1.3724	0.8055	0.5668	2.055	–14.60	–15.34	–12.93	13.66	0.18
N7–C7	1.4610	0.9074	0.5528	1.570	–11.32	–10.32	-7.97	6.97	0.29
N7–C8	1.3550	0.8773	0.4787	2.093	–15.65	–15.96	–12.24	12.54	0.30
N9–C4	1.3498	0.7683	0.5830	2.244	–18.78	–18.47	–15.30	14.98	0.21
N9–C8	1.3361	0.7480	0.5882	2.367	–18.88	–18.26	–16.44	15.82	0.11
O6–C6	1.2210	0.7608	0.4610	2.910	–37.91	–28.89	–24.86	15.84	0.16
C1–H11	0.9780	0.7300	0.3603	1.817	–16.80	–17.35	–16.65	17.21	0.04
C1–H12	0.9815	0.7305	0.3587	1.841	–17.13	–17.47	–17.05	17.39	0.02
C1–H13	0.9816	0.7286	0.3611	1.836	–16.46	–17.02	–16.95	17.51	0.04
C2–H2	0.9501	0.7436	0.3350	1.831	–18.94	–18.75	–17.71	17.52	0.06
C3–H31	0.9805	0.7230	0.3718	1.740	–14.15	–16.15	–15.25	17.24	0.06
C3–H32	0.9814	0.7279	0.3629	1.746	–15.39	–16.64	–15.42	16.68	0.08
C3–H33	0.9792	0.7248	0.3678	1.711	–14.70	–16.09	–15.04	16.43	0.07
C4–C5	1.3833	0.7135	0.6711	2.146	–18.26	–16.16	–13.72	11.62	0.18
C5–C6	1.4273	0.6775	0.7510	2.084	–16.80	–16.35	–13.16	12.70	0.24
C7–H71	0.9869	0.7579	0.3413	1.805	–15.96	–17.77	–16.76	18.57	0.06
C7–H72	0.9747	0.7353	0.3575	1.781	–17.56	–17.07	–16.98	16.50	0.05
C7–H73	0.9772	0.7304	0.3614	1.714	–15.80	–16.21	–15.29	15.70	0.06
C8–H8	0.9506	0.7376	0.3438	1.864	–18.25	–18.67	–17.61	18.05	0.06
O1w–H1w	0.9830	0.8199	0.1585	1.602	–42.09	–29.38	–28.75	16.04	0.02
O1w–H2w	0.9830	0.8139	0.1662	1.639	-39.26	–29.24	–28.10	18.07	0.04

9. References

SI-1 H. Biltz and H. Rakett, *Ber. Dtsch. Chem. Ges.*, 1928, **61**, 1409–1422.

SI-2 A. Makhloufi, W. Frank and C. Ganter, *Organometallics*, 2012, **31**, 7272–7277.

SI-3 Bruker AXS Inc., SAINT, version 6.01, Bruker AXS Inc., Madison, WI, USA, 2001.

SI-4 Bruker AXS Inc., SADABS, Area Detector Absorption Program, Bruker AXS Inc., Madison, WI, USA, 1996

SI-5 L. Krause, R. Herbst-Irmer, G. M. Sheldrick and D. Stalke, *J. Appl. Crystallogr.*, 2015, **48**, 3–10.

SI-6 G. M. Sheldrick, *Acta Crystallogr. Sect. A*, 2008, **64**, 112–122.

SI-7 G. M. Sheldrick, *Acta Crystallogr. Sect. C*, 2015, **71**, 3–8.

SI-8 L. J. Farrugia, *J. Appl. Cryst.*, 2012, **45**, 849–854.

SI-9 O. V. Dolomanov, L. J. Bourhis, R. J. Gildea, J. A. K. Howard and H. Puschmann, *J. Appl. Cryst.*, 2009, **42**, 339–341.

SI-10 S. Alvarez, *Dalton Trans.*, 2013, **42**, 8617–8636.

SI-11 B. Cordero, V. Gómez, A. E. Platero-Prats, M. Revès, J. Echeverría, E. Cremades, F. Barragán and S. Alvarez, *Dalton Trans.*, 2008, 2832–2838.

SI-12 D. M. Gil, J. Echeverría and S. Alvarez, *Inorg. Chem.*, 2022, **61**, 9082–9095.

SI-13 P. R. Spackman, M. J. Turner, J. J. McKinnon, S. K. Wolff, D. J. Grimwood, D. Jayatilaka and M. A. Spackman, *J. Appl. Cryst.*, 2021, **54**, 1006–1011.

SI-14 C. Jelsch, B. Guillot, A. Lagoutte and C. Lecomte, *J. Appl. Cryst.*, 2005, **38**, 38–54.

SI-15 A. O. Madsen and A. A. Hoser, *J. Appl. Cryst.*, 2014, **47**, 2100–2104.

SI-16 W.F. Kuhn, *Acta Cryst*., 1992, **A48**, 80-98.

SI-17 N. K. Hansen and P. Coppens, *Acta Cryst.*, 1978, **A34**, 909–921.